

# Studying Short-Range Correlations with Real Photon Beams at GlueX

H. Marukyan

A. I. Alikhanian National Science Laboratory  
(Yerevan Physics Institute), 0036 Yerevan, Armenia

M. Patsyuk (Spokesperson)

Joint Institute for Nuclear Research, Dubna, Russia

H. Gao (Spokesperson)

Duke University, Durham, North Carolina 27708, USA

M. Kamel, L. Guo

Florida International University, Miami, Florida 33199, USA

D. G. Ireland, K. Livingston, B. Mckinnon, P. Pauli, A. Thiel  
University of Glasgow, Glasgow G12 8QQ, United Kingdom

F. Nerling

GSI Helmholtzzentrum für Schwerionenforschung GmbH,  
D-64291 Darmstadt, Germany

T. Britton, M. M. Dalton, A. Deur, H. Egiyan, S. Furletov, D.W. Higinbotham,  
D. Lawrence, D. Mack, M. McCaughan, L. Pentchev, A. Somov (Spokesperson),  
H. Szumila-Vance (Spokesperson), S. Taylor, B. Zihlmann  
Thomas Jefferson National Accelerator Facility,  
Newport News, Virginia 23606, USA

A. Ashkenazi, R. Cruz-Torres, A. Denniston, C. Fanelli, O. Hen (Spokesperson\*),  
D. Nguyen, A. Papadopoulou, J. R. Pybus, E.P. Segarra  
Massachusetts Institute of Technology, Cambridge, Massachusetts 02139, USA

D. Dutta (Spokesperson)

Mississippi State University, Mississippi State, Mississippi 29762, USA

V. Berdnikov, D. Romanov, S. Somov  
National Research Nuclear University Moscow Engineering Physics Institute,  
Moscow 115409, Russia

C. Salgado  
Norfolk State University, Norfolk, Virginia 23504, USA

R. Pedroni  
North Carolina A&T State University, Greensboro, North Carolina 27411, USA

T. Black, L. Gan  
University of North Carolina at Wilmington,  
Wilmington, North Carolina 28403, USA

A. Beck, I. Korover, and S. Maytal-Beck  
Nuclear Research Center Negev, Beer-Sheva 84190, Israel

M. Amaryan, F. Hauenstein, L.B. Weinstein (Spokesperson)  
Old Dominion University, Norfolk, Virginia 23529, USA

W. Brooks, H. Hakobyan, S. Kuleshov, C. Romero  
Universidad Técnica Federico Santa María, Casilla 110-V Valparaíso, Chile

B. Schmookler  
State University of New York at Stony Brook, New York, 11794

G. Johansson, E. Piassetzky (Spokesperson)  
Tel-Aviv University, Tel Aviv 69978, Israel

W. J. Briscoe, S. Fegan, S. Ratliff, A. Schmidt (Spokesperson), E. Seroka,  
P. Sharp, I. I. Strakovsky  
The George Washington University, Washington, D.C. 20052, USA

Theory Support

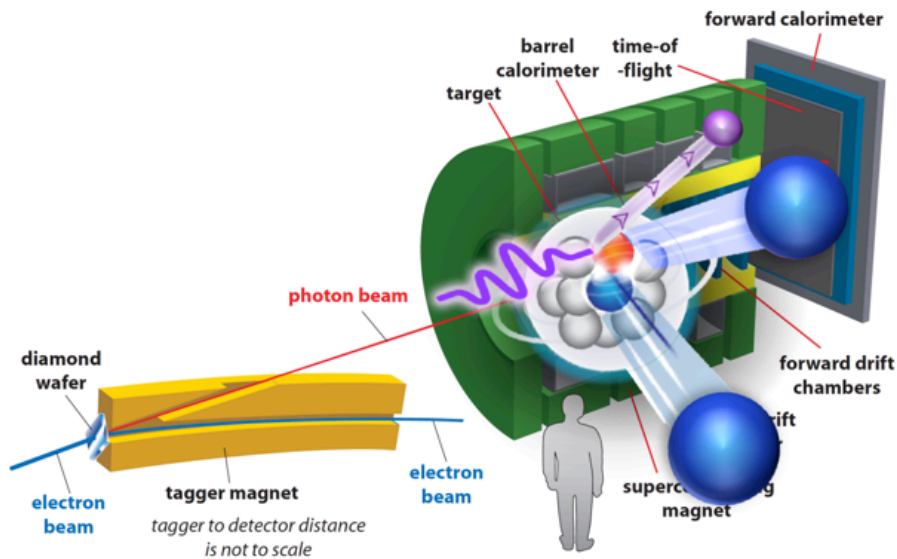
M. Strikman	Pennsylvania State University, State College, PA.
G.A. Miller	University of Washington, Seattle, WA.
A.B. Larionov	Frankfurt Institute for Advanced Studies (FIAS), and National Research Centre “Kurchatov Institute”, Moscow, Russia.
M. Sargsian	Florida International University, Miami, FL.
L. Frankfurt	Tel-Aviv University, Tel Aviv, Israel.

---

\*Contact Person: [hen@mit.edu](mailto:hen@mit.edu)

## Abstract

The past few years has seen tremendous progress in our understanding of short-range correlated (SRC) pairing of nucleons within nuclei, much of it coming from electron scattering experiments leading to the break-up of an SRC pair. The interpretation of these experiments rests on assumptions about the mechanism of the reaction. These assumptions can be directly tested by studying SRC pairs using alternate probes, such as real photons. We propose a 30-day experiment using the Hall D photon beam, nuclear targets, and the GlueX detector in its standard configuration to study short-range correlations with photon-induced reactions. Several different reaction channels are possible, and we project sensitivity in most channels to equal or exceed the 6 GeV-era SRC experiments from Halls A and B. The proposed experiment will therefore decisively test the phenomena of  $np$  dominance, the short-distance  $NN$  interaction, and reaction theory, while also providing new insight into bound nucleon structure and the onset of color transparency.



## 1 Introduction

Since the 1950s much effort has been devoted to understanding the detailed characteristics and origin of the nucleon-nucleon interaction, and how it forms atomic nuclei. The development of modern superconducting accelerators—with high energy, high intensity and high duty factor—has enabled scattering experiments that resolve the structure and dynamics of both individual nucleons and nucleon pairs in nuclei, allowing significant progress. While many breakthroughs have been made, much still remains to be understood.

Early measurements of inclusive ( $e, e'$ ) and single proton knockout ( $e, e'p$ ) processes helped establish the shell-structure of nuclei and probe properties of nucleons bound in different nuclear shells [1–3]. While lending credence to many shell model predictions, these measurements also revealed that in nuclei ranging from lithium to lead, proton-knockout cross-sections are only 60%–70% of the mean-field one-body-based theoretical expectation [4,5], highlighting the need to consider higher order two-body effects that go beyond the traditional mean-field approximation.

Electron-scattering experiments, analyzed within a high-resolution theoretical framework, suggest that about 20% of the nucleons in nuclei are part of strongly interacting close-proximity nucleon pairs, with large relative ( $k_{rel} > k_F \approx 250$  MeV/c) and small center-of-mass (C.M.) momenta ( $k_{CM} < k_F$ ). These are referred to as short-range correlated (SRC) pairs [6–9]. Nucleons that are

part of SRC pairs are absent in the one-body shell-model description of the data. Their formation can therefore explain some of the discrepancy between the measured and calculated single-proton knockout cross-sections [5,10] and have wide-spread implications for different phenomena in nuclear-, particle- and astro-physics.

A large part of our understanding of SRC pairs comes from measurements of exclusive two-nucleon knockout reactions ( $e, e'NN$ ). In these experiments, a high-energy electron scatters off the nucleus, leading to the knockout of a nucleon with large missing momentum that is balanced by the emission of a single recoil nucleon, leaving the residual  $A - 2$  system with both low momentum and low excitation energy.

The very successful JLab SRC program resulted in multiple experimental papers published in Nature [11,12], Science [13,14], PRL [15–18], Physics Letters B [19] and more, with new results currently undergoing peer-review [20,21]. These results showed that almost all high-momentum nucleons in nuclei belong to SRC pairs [14–17,22,23]. For relative momenta between 300–600 MeV/ $c$  (just above  $k_F$ ), neutron-proton ( $np$ ) SRC pairs predominate over proton-proton ( $pp$ ) and neutron-neutron ( $nn$ ) pairs by a factor of about 20, in both light and heavy nuclei [13,16,17]. This phenomenon, commonly referred to as “ $np$ -dominance,” [12–17,22,23], is driven by the tensor nature of the  $NN$  interaction in the quoted momentum range [24–26] and indicates that increasing the fraction of neutrons in a nucleus increases the fraction of protons that are part of SRC pairs [12,27,28].

These experimental findings inspired a broad complementary program of theoretical and phenomenological studies of SRCs and their impact on various nuclear phenomena, including the internal structure of nucleons bound in nuclei [11,29–32], neutrinoless double beta decay matrix elements [33–39], nuclear charge radii [40], and the nuclear symmetry energy and neutron star properties [9,41,42].

However, almost all of our understand of SRC comes from electron scattering, with only a single proton scattering  $C(p, ppn)$  measurement [23]. Thus, the interpretation of these experimental results relies on an assumed electron interaction mechanism at large momentum transfers (detailed in section 2 below). Different assumptions could lead to different interpretations. It is crucial to study SRCs with different, non-electron, probes, in order to validate the reaction mechanism assumptions and the connection between the experimental results and their interpretation in terms of SRC pairs.

This proposal describes an experiment to study SRCs using photo-production reactions with real photons on nuclear targets to determine the probe-dependence of SRC measurements. The new data will complement the above-mentioned electron scattering studies and yield stringent constraints on possible reaction mechanisms that could complicate the interpretation of the data. Photo-nuclear reactions have significantly different sensitivity to meson exchange currents, are dominated by the transverse response function with backward emitted recoil nucleons (as oppose to both longitudinal and transverse response functions and forward emitted recoil nucleons in  $x_B > 1$  electron scattering kinematics). If the reaction mechanisms at these high momentum transfer reactions ( $Q^2, |t|, |u| > 2 \text{ GeV}^2$ ) are indeed understood to the expected level, we should be able to confirm the observed neutron-proton pair dominance and the  $A$ -dependence of SRC-pair abundances through this experiment. We note that nuclear targets have been considered as part of the future plan for the GlueX Detector, as laid out by the recent GlueX collaboration white paper [43].

We propose a 30-day measurement using the real photon beam in Hall D, three nuclear targets ( $d$ ,  $^4\text{He}$ , and  $^{12}\text{C}$ ), and the GlueX detector in its standard configuration. The main goal of the experiment will be to study short-range correlations using photon-induced reactions. The experiment can additionally provide information on bound nucleon structure (discussed in section 3) and color-transparency (discussed in section 4).

## 2 Recent progress in the quantitative study of SRCs

The study of short-range correlations is a broad subject. It covers a large body of experimental and theoretical work, as well as phenomenological studies of the implications of SRCs for various phenomena in nuclear, particle and astro-physics. The discussion below is focused primarily on recent experimental activities co-led by the spokespersons, and theoretical developments that are most relevant for the objectives of the current proposal. A full discussion of SRC physics is available in a recent RMP review [6], as well as in a theory-oriented review [7].

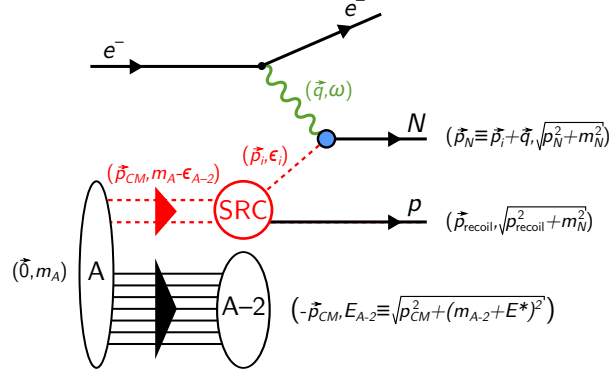


Figure 1: Diagrammatic representation and kinematics of the triple-coincidence  $A(e, e'Np)$  reaction within the SRC breakup model. Dashed red lines represent off-shell particles. Open ovals represent un-detected systems. Solid black lines represent detected particles. The momentum and energy of the particles are also indicated.

Previous studies of SRCs have used measurements of Quasi-Elastic (QE) electron scattering at large momentum-transfer, see Fig. 1. Within the single-photon exchange approximation, electrons scatter from the nucleus by transferring a virtual photon carrying momentum  $\vec{q}$  and energy  $\omega$ . In the one-body view of QE scattering, the virtual photon is absorbed by a single off-shell nucleon with initial energy  $\epsilon_i$  and momentum  $\vec{p}_i$ . If the nucleon does not re-interact as it leaves the nucleus, it will emerge with momentum  $\vec{p}_N = \vec{p}_i + \vec{q}$  and energy  $E_N = \sqrt{p_N^2 + m_N^2}$ . Thus, we can approximate the initial momentum and energy of that nucleon using the measured missing momentum,  $\vec{p}_i \approx \vec{p}_{\text{miss}} \equiv \vec{p}_N - \vec{q}$ , and missing energy,  $\epsilon_i \approx m_N - \epsilon_{\text{miss}} \equiv \epsilon_N - \omega$ . When  $\vec{p}_{\text{miss}} > k_F$ , the knockout nucleon is expected to be part of an SRC pair [6–9, 14, 16, 22]. The knockout of one nucleon from the pair should therefore be accompanied by the simultaneous emission of the second (recoil) nucleon with momentum  $\vec{p}_{\text{recoil}} \approx -\vec{p}_{\text{miss}}$ . At the relevant high- $Q^2$  of our measurements ( $> 1.7\text{--}2.0$  GeV/c), the differential  $A(e, e'p)$  cross-sections can be approximately factorized as [3, 44]:

$$\frac{d^6\sigma}{d\Omega_{k'} d\epsilon_{k'} d\Omega_N d\epsilon_N} = p_N \epsilon_N \cdot \sigma_{ep} \cdot \mathcal{S}(p_i, \epsilon_i), \quad (1)$$

where  $k' = (k', \epsilon_{k'})$  is the final electron four-momentum,  $\sigma_{ep}$  is the off-shell electron-nucleon cross-section [44], and  $\mathcal{S}(p_i, \epsilon_i)$  is the nuclear spectral function that defines the probability for finding a nucleon in the nucleus with momentum  $p_i$  and energy  $\epsilon_i$ . Different models of the  $NN$  interaction can produce different spectral functions that lead to different cross-sections. Therefore, exclusive nucleon knockout cross-sections analyzed with this method are sensitive to the  $NN$  interaction.

In the case of two-nucleon knockout reactions, the cross-section can be factorized in a similar manner to Eq. 1 by replacing the single-nucleon spectral function with the two-nucleon decay function  $\mathcal{D}_A(p_i, p_{\text{recoil}}, \epsilon_{\text{recoil}})$  [9, 22, 45]. The latter represents the probability for a hard knockout of a nucleon with initial momentum  $\vec{p}_i$ , followed by the emission of a recoil nucleon with momentum  $\vec{p}_{\text{recoil}}$ .  $\epsilon_{\text{recoil}}$  is the energy of the  $A - 1$  system, composed of the recoil nucleon and residual  $A - 2$  nucleus.

Non-QE reaction mechanisms that add coherently to the measured cross-section can lead to high- $p_{\text{miss}}$  final states that are not due to the knockout of nucleons from SRC pairs, thus breaking the factorization shown in Eq. 1. To address this, the measurements discussed here are carried out at anti-parallel kinematics with  $p_{\text{miss}} \geq 300 \text{ MeV}/c$ ,  $Q^2 \equiv q^2 - \omega^2 \geq 1.7 \text{ (GeV}/c)^2$ , and  $x_B \equiv Q^2/2m_N\omega \geq 1.2$ , where such non-QE reaction mechanisms were shown to be suppressed [6–9, 46, 47].

For completeness, we note that from a theoretical standpoint, the reaction diagram shown in Fig. 1 can be viewed as a ‘high-resolution’ starting point for a unitary-transformed calculation [48]. Such calculations would soften the input  $NN$  interactions and turn the electron scattering operators from one-body to many-body. This ‘unitary-freedom’ does not impact cross-section calculations but does make the extracted properties of the nuclear ground-state wave-function (e.g. the spectral function) depend on the assumed interaction operator. This discussion focuses on the high-resolution electron interaction model of Fig. 1, as it constitutes the simplest reaction picture that is consistent with both the measured observables [6–9] and various reaction and ground-state ab-initio calculations [49].

## 2.1 Short-Distance $NN$ Interaction at the Generalized Contact Formalism

Precision SRC studies are only feasible if one has the ability to quantitatively relate experimental observables to theoretical calculations, ideally ones starting from the fundamental  $NN$  interaction and accounting for all relevant reaction mechanisms. This is a challenging endeavor, as un-factorized ab-initio calculations of high- $Q^2$  nucleon knockout cross-sections are currently unfeasible for  $A > 3$  nuclei. Even the simple factorized approximation of Eq. 1 requires knowledge of the nuclear spectral function that, at the moment, cannot be calculated using ab-initio techniques for high-momentum states in finite nuclei [49].

To help overcome this challenge, the effective two-body Generalized Contact Formalism (GCF) was recently developed, [50–52] that allows calculating factorized cross-sections, within a scale-separated approximation, using the underlying  $NN$  interaction as input [17, 51]. This is done by providing a factorized model of the short-distance / high-momentum part of the many-body nuclear wave function leveraging the separation between the energy scales of the  $A - 2$  system (low energy) and the SRC pair (medium energy). Considering a high- $Q^2$  scattering reactions such as in Fig. 1 adds a third energy scale of the virtual photon (high-energy) that justifies the factorized approximation of Eq. 1.

The GCF provides a consistent model for nuclear two-body momentum distribution at high-momenta and at short-distance, as well as for two-body continuum states of the nuclear spectral and decay functions. Recent studies of the GCF:

- Demonstrated its ability to reproduce many-body ab-initio calculated nucleon momentum distributions in nuclei from  $^4\text{He}$  to  $^{40}\text{Ca}$ , above  $k_F$ , to  $\approx 10\%$  accuracy [50];
- Extracted consistent SRC abundances (i.e., nuclear contacts) from ab-initio calculations of two-nucleon distributions in both coordinate and momentum space and from experimental data [50]; and
- Derived a new factorized expression for the nuclear correlation function with implications for calculations of double beta decay matrix elements [33] and demonstrated its relation to single-nucleon charge distribution measurements [40].

The main application of the GCF germane to this proposal is the modeling of the nuclear spectral and decay functions [51], allowing calculations of nucleon knockout cross-sections. For example, using Eq. 1 and the reaction model of Fig. 1, the  $A(e, e'NN)$  cross-section can be expressed within the

GCF as [17]:

$$\frac{d^8\sigma}{dQ^2 dx_B d\phi_k d^3\vec{p}_{CM} d\Omega_{\text{recoil}}} = K \cdot \sigma_{eN} \cdot n(\vec{p}_{CM}) \cdot \left[ \sum_{\alpha} C_{\alpha} \cdot |\tilde{\varphi}^{\alpha}(|\vec{p}_{CM} - 2\vec{p}_{\text{recoil}}|)|^2 \right], \quad (2)$$

where subscripts ‘ $N$ ’ and ‘recoil’ stand for the leading and recoil nucleon respectively,  $K$  is a kinematic term, (detailed in Ref. [17]),  $\sigma_{eN}$  is the off-shell electron-nucleon cross-section, and  $\alpha$  represents the spin and isospin quantum numbers of SRC pairs.  $\tilde{\varphi}^{\alpha}$ ,  $n(\vec{p}_{CM})$ , and  $C_{\alpha}$  respectively describe the relative motion, CM motion, and abundances of SRC pairs with quantum numbers  $\alpha$ . The functions  $\tilde{\varphi}^{\alpha}$  are universal SRC pair relative momentum distributions, obtained by solving the zero-energy two-body Schrödinger equation of an  $NN$  pair in quantum state  $\alpha$  using an input  $NN$  potential model.  $n(\vec{p}_{CM})$  is the SRC pair CM momentum distribution, given by a three-dimensional Gaussian with width of  $150 \pm 20$  MeV/ $c$  [18, 53, 54].  $C_{\alpha}$  are the nuclear contact terms that determine the relative abundance of SRC pairs in quantum state  $\alpha$ . These are obtained through the analysis of ab-initio many-body calculations of two-nucleon densities [50, 52, 55].

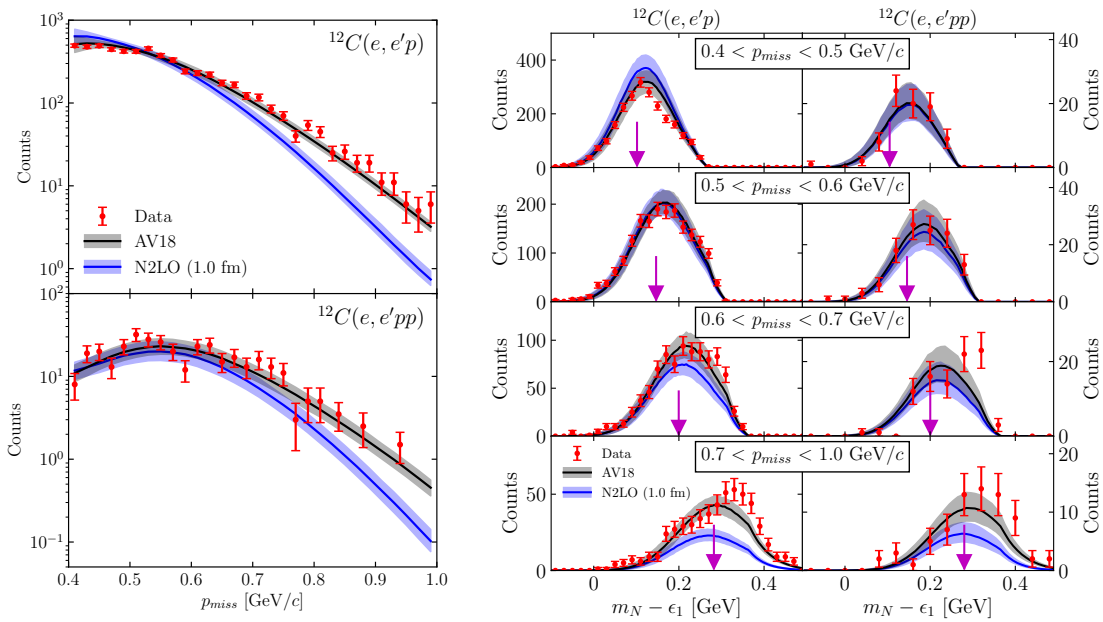


Figure 2: Left panel: the  $p_{\text{miss}}$  dependence of the  $^{12}\text{C}(e, e'p)$  (top) and  $^{12}\text{C}(e, e'pp)$  (bottom) event yields. Points show the measured data. Bands show the GCF calculations using the N2LO(1.0fm) (blue) and AV18 (black) interactions. Right panel: the  $\epsilon_{\text{miss}}$  dependence of the  $^{12}\text{C}(e, e'p)$  (left column) and  $^{12}\text{C}(e, e'pp)$  (right column) event yields in four different ranges of  $p_{\text{miss}}$ . The purple arrow indicates the expected  $\epsilon_{\text{miss}}$  for standing SRC pair breakup with a missing-momentum that is equal to the mean value of the data.

Ref. [17] shows the first comparisons between the prediction of Eq. 2 and measured  $A(e, e'Np)$  cross-section ratios. In Figs. 2 and 3 we showcase our most recent results, where Eq. 2 is used to calculate the individual  $(e, e'p)$  and  $(e, e'pp)$  cross-sections in the kinematics of our SRC measurements. The calculation was done using two  $NN$  interaction models to obtain  $\tilde{\varphi}^{\alpha}$ : the phenomenological AV18 [56], and Chiral EFT-based local N2LO(1.0 fm) [57]. Nuclear contacts  $C_{\alpha}$  and width of the CM momentum distribution were obtained from theoretical calculations [50, 52–55] and nuclear transparency and single-charge exchange reaction effects were accounted for as detailed in the on-line supplementary materials of Ref. [17], using the calculations of Ref. [46]. The model systematic

uncertainty is determined from the uncertainties in the GCF input parameters and reaction effects correction factors.

The left panel of Fig. 2 shows the  $p_{\text{miss}}$  dependence of the measured and GCF-calculated  $^{12}\text{C}(e, e'pp)$  and  $^{12}\text{C}(e, e'p)$  event yields for the two interactions. The AV18 interaction is observed to describe both  $(e, e'p)$  and  $(e, e'pp)$  data over the entire measured  $p_{\text{miss}}$  range. The N2LO(1.0 fm) interaction agrees with the data up to its cutoff and, as expected, decreases exponentially above it.

The right panel of Fig. 2 shows the  $\epsilon_{\text{miss}}-p_{\text{miss}}$  correlation for the  $^{12}\text{C}(e, e'pp)$  and  $^{12}\text{C}(e, e'p)$  reactions. The average value of  $m_N - \epsilon_1$  is observed to increase with  $p_{\text{miss}}$ , peaking at the expected value for the breakup of a standing SRC pair (indicated by the purple arrows) for both reactions. The GCF calculations follow the same trend. However, the AV18 interaction agrees with the data over the entire  $\epsilon_{\text{miss}}-p_{\text{miss}}$  range, while the chiral interactions under predict at the highest  $p_{\text{miss}}$ .

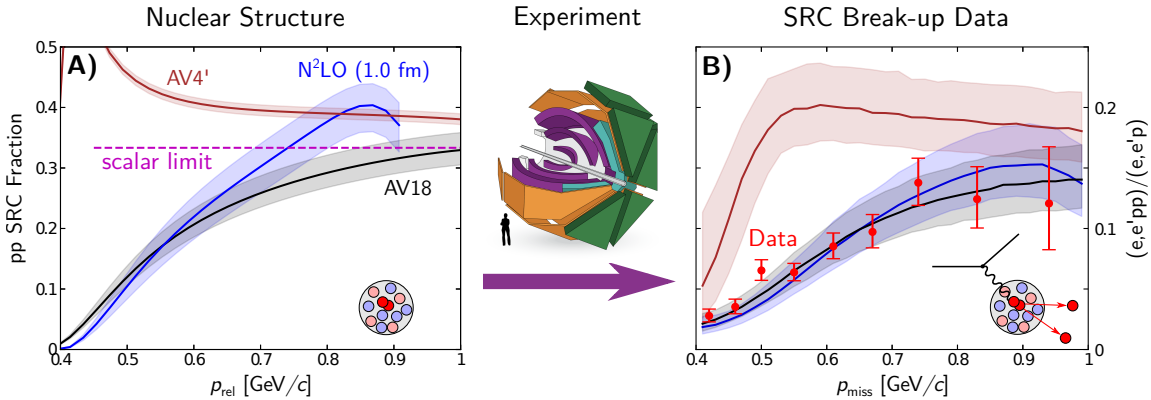


Figure 3: A: the  $pp$  pair fraction in  $^{12}\text{C}$  as predicted by GCF using AV18, AV4', and Chiral N2LO(1.0 fm) interactions. B: the ratio of  $^{12}\text{C}(e, e'pp)$  to  $^{12}\text{C}(e, e'p)$  event yields for data (red points) and GCF (bands), including all experimental effects. Both the AV18 and N2LO(1.0 fm) interactions are consistent with data, and show an increase from a tensor-dominated regime at  $p_{\text{miss}} = 0.4$  GeV/c to scalar spin-independent regime approaching  $p_{\text{miss}} = 1$  GeV/c. The AV4' interaction, which has no tensor component, leads to predictions that are inconsistent with data.

Fig. 3 considers the  $^{12}\text{C}(e, e'pp)/^{12}\text{C}(e, e'p)$  yield ratio, a measure of the impact of the tensor force in the  $NN$  interaction. In this figure, the AV18 and the chiral N2LO(1.0 fm) interactions are compared to the AV4' interaction, which does not include a tensor force. The right panel shows the data yield ratio as well as the GCF-calculated yield ratio. Both the data, and the calculations with the AV18 and N2LO(1.0 fm) interactions show the  $pp$  fraction increasing with  $p_{\text{miss}}$ , consistent with a transition from tensor- to scalar-dominated regions of the interaction [16]. By contrast, the calculation with the AV4' interaction over-predicts the fraction of  $pp$  pairs observed in the data.

The left panel shows the fraction of  $pp$  pairs in  $^{12}\text{C}$  as predicted by the GCF formalism as a function of  $p_{\text{rel.}} \equiv \frac{1}{2}|\vec{p}_{\text{miss}} - \vec{p}_{\text{recoil}}|$ . The AV18 and N2LO(1.0 fm) interactions approach limit predicted by a purely spin-independent interaction. The AV4' interaction, without a tensor force, predicts a  $pp$  fraction above this scalar limit.

We note that our confidence in these results is also supported by the fact that the GCF-based calculations describe well numerous other measured kinematical distributions not shown here due to a lack of space. Thus, the results presented here showcase the use of high- $Q^2$  electron scattering data to quantitatively study the nuclear interaction at very large momenta.

It is interesting to note that for the AV18 interaction, we observe good agreement with the data up to 1 GeV/c, which corresponds to SRC configurations with nucleons separated by a distance smaller than their radii [58]. As discussed below, previous studies indicated that in such extreme conditions the internal quark-gluon structure of SRC nucleons can well be modified as compared with

that of free nucleons [6, 11, 59–61]. The ability of the AV18-based GCF calculation to reproduce our data over the entire measured  $\epsilon_{\text{miss}}\text{-}p_{\text{miss}}$  range suggests that such modifications do not significantly impact the effective modeling of the nuclear interaction, offering support for using point-like nucleons as effective degrees of freedom for modeling of nuclear systems up to very high densities.

## 2.2 Two-Nucleon Knockout Reactions

The above-mentioned results constitute some of the most advanced, ongoing (i.e. unpublished), analysis that utilizes the scale-separated GCF to calculate factorized nucleon-knockout cross-sections using different models of the  $NN$  interaction. These studies are made possible by the vast progress made in the study of SRCs using hard knockout reactions over the last decade. Below, we review key published results from initial measurements of nuclei from  ${}^4\text{He}$  to  ${}^{208}\text{Pb}$ .

### 2.2.1 $np$ -SRC dominance and the tensor interaction

First measurements of exclusive SRC pair breakup reactions focused primarily on probing the isospin structure of SRC pairs. These experiments were initially done at BNL using hadronic (proton) probes on  ${}^{12}\text{C}$ , and continued at JLab with leptonic (electron) probes on  ${}^4\text{He}$ ,  ${}^{12}\text{C}$ ,  ${}^{27}\text{Al}$ ,  ${}^{56}\text{Fe}$  and  ${}^{208}\text{Pb}$ .

Focusing on a missing momentum range of 300–600 MeV/ $c$ , comparisons of the measured  $A(e, e'p)$  and  $A(e, e'pN)$  cross-section indicated that the full single-proton knockout cross-section is exhausted by the two-nucleon knockout cross-sections, i.e., the data were consistent with every  $(e, e'p)$  event having the correlated emission of a recoil nucleon [14, 16, 17, 22]. A common interpretation of these results is that the nucleon momentum distribution above  $k_F$  is dominated by nucleons that are members of SRC pairs.

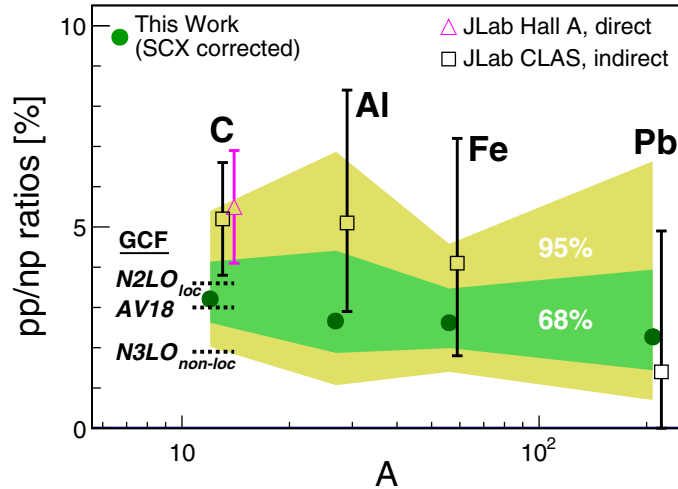


Figure 4:  $np$ -SRC dominance in nuclei from  ${}^{12}\text{C}$  to  ${}^{208}\text{Pb}$  extracted from  $A(e, e'Np)$  and  $A(e, e'p)$  measurements [13, 14, 17], compared with GCF calculations [17].

Furthermore, the measured  $A(e, e'pn)$  and  $A(e, e'np)$  cross-sections were found to be significantly higher than the  $A(e, e'pp)$  cross-section. This finding, consistently observed in all measured nuclei, was interpreted as evidence for  $np$ -SRC pairs being about  $20\times$  more abundant than  $pp$ -SRC pairs (Fig. 4). From a theoretical standpoint, this  $np$ -SRC predominance was interpreted as resulting from the dominance of the tensor part of the  $NN$  interaction at the probed sub-fm distances [6, 7, 24–26] (see Fig. 5).

It should be pointed out that, on average, the tensor part of the  $NN$  interaction is long-ranged and small compared to the dominant scalar part. However, studies of the deuteron suggest that

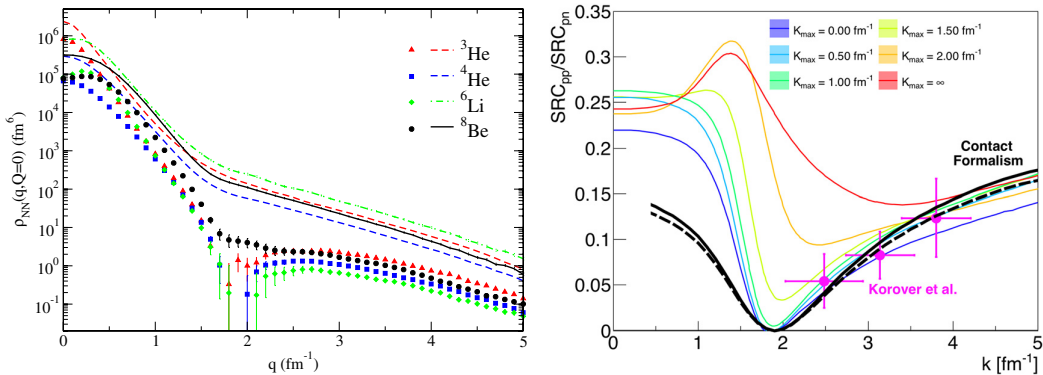


Figure 5: Left: calculated  $pp$  (points) and  $np$  (lines) stationary pair momentum densities in light nuclei [24]. Right: measured and calculated  ${}^4\text{He}$   $pp/np$  pair density ratios as a function of the pair relative momentum [50].

its second order effect, viewed as a two-pion exchange term, becomes important in the momentum range where the scalar force approaches zero ( $\approx 0.75\text{--}1$  fm) [6]. At shorter distances, i.e., higher relative momenta, the dominance of the tensor interaction is expected to be washed out, which would manifest in an increase in the fraction of  $pp$ -SRC pairs with much larger missing momentum. Fig. 5 shows the measured increase in the fraction of  $pp$ -SRC pairs [16], which is overall consistent with theoretical expectation based on calculations of two-nucleon momentum distributions [55] and their GCF representation [50]. The large error bars of the  ${}^4\text{He}$  data makes it hard to draw any conclusive quantitative conclusions on the  $NN$  interaction beyond the tensor limit. However, as shown above, the combination of improved data, and recent theoretical developments (such as the GCF), allows addressing such issues.

### 2.2.2 SRC pair C.M. motion

Measurements of exclusive two-nucleon knockout reactions allow us to probe the detailed characteristics of SRC pairs, going beyond their isospin structure. One such property of interest is the C.M. motion of SRC pairs. It is a measure of the interaction of the pair with the ‘mean-field’ potential created by the residual  $A - 2$  system. Its magnitude, as compared with the relative motion of the nucleons in the pairs, is key for establishing effective scale-separated models of SRCs such as the GCF presented above and serves as an input for theoretical calculations.

The CM motion of SRC pairs is expected to be described by a gaussian distribution, defined by its width. Therefore, experiments often report on their extraction of the C.M. gaussian width,  $\sigma_{CM}$ .

Fig. 6 shows new results from the extraction of the  $\sigma_{CM}$  for  $pp$ -SRC pairs from an analysis of  $A(e, e'pp)$  data, led by graduate student E. Cohen and the spokespersons [18]. The extracted C.M. momentum distribution for the measured nuclei was observed to be consistent with a Gaussian distribution in each direction, as expected. The extracted values of  $\sigma_{CM}$  were observed to vary between 140 and 160 MeV/ $c$ , and are consistent with a constant within experimental uncertainties.

Comparisons with theory predictions show good agreement with either a simple Fermi-gas model prediction (where the  $NN$  pairs are formed from two randomly chosen nucleons, each following a Fermi-Gas momentum distribution with  $k_F = 250$  MeV/ $c$ ) or more realistic mean-field calculations [53, 54]. Interestingly, the data seem to be higher than the mean-field predictions that assume all  $NN$  pairs can form SRC pairs, but lower than the most restrictive  ${}^1S_0$  calculation (i.e., assuming only mean-field  $pp$  pairs in a relative  ${}^1S_0$  state can form  $pp$ -SRC pairs). This indicates some selectivity in the SRC pair formation process and was suggested to provide insight to their quantum numbers [18, 54, 62].

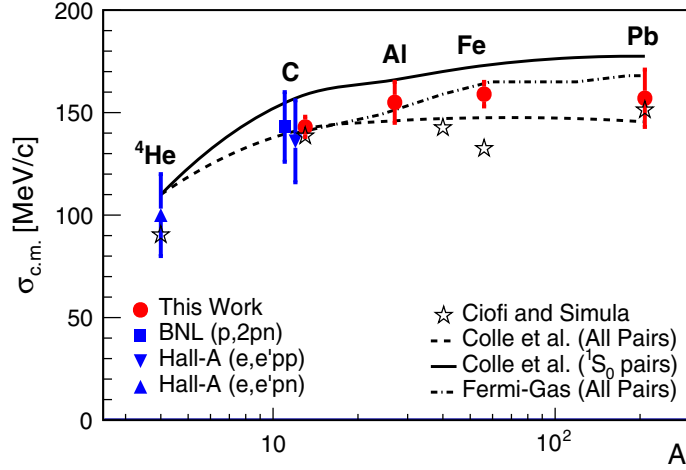


Figure 6: Width of  $pp$ -SRC pairs C.M. momentum distribution, extracted from  $A(e, e'pp)$  data (red circles) [18], compared with previous extractions (blue points). The width is extracted assuming a 3D gaussian for the C.M. distribution, defined by its width,  $\sigma_{CM}$ . The lines and stars show mean-field theory predictions [53, 54].

### 2.3 Final State Interactions in Hard QE Scattering

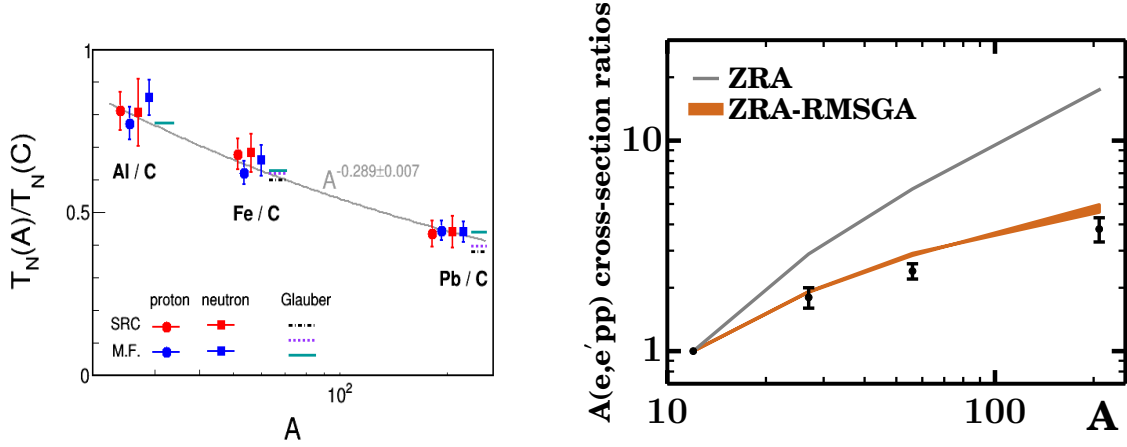


Figure 7: Nucleon transparency ratios for nuclei relative to  $^{12}\text{C}$ , extracted from single-nucleon knockout measurements (left) [20], and calculations of the two-nucleon knockout reaction [62] using Glauber theory (right).

The results presented above in sections 2.1 and 2.2 require corrections for reaction effects such as final-state interactions (FSI) and single-charge exchange (SCX). Therefore, understanding the impact of such reaction mechanism effects on hard electron QE scattering cross-sections is crucial for the interpretation of measurements in general, and specifically their relation to ground-state properties of nuclei. In high- $Q^2$  reactions, one may use the Generalized Eikonal approximation within a Glauber-framework to perform quantitative estimations of reaction effects such as FSI and SCX. However, additional experimental verification of this approach in the kinematics of our measurements are needed. Several measurements of the nuclear transparency of proton knockout in  $(e, e'p)$  and  $(e, e'pp)$  reactions in SRC kinematics were compared them with theoretical calculations

using the Glauber approximation [19,62] (Fig. 7, right). The experimentally extracted transparency ratios showed good agreement with Glauber calculations. Recently, this work was extended to measurements of neutron knockout ( $e, e'n$ ) reactions in both SRC and Mean-Field kinematics [20] (Fig. 7 top panel). The extracted transparency for both proton and neutron knockout in mean-field and SRC kinematics were observed to agree with each other and with Glauber calculations. The combined nuclear mass dependence of the data is consistent with power-law scaling of  $A^\alpha$  with  $\alpha = -0.285 \pm 0.011$ , which is consistent with nuclear surface dominance of the reactions.

## 2.4 Nuclear Asymmetry Dependence in SRCs

The predominance of  $np$ -SRC pairs leads to interesting phenomena in asymmetric nuclei. Without SRC pairs, neutrons in neutron-rich nuclei should have a higher Fermi momentum and thus a higher average momentum and kinetic energy than the minority protons. However, since the high-momentum tail of the momentum distribution is dominated by  $np$ -pairs, there should be equal numbers of protons and neutrons above  $k_F$ . Therefore, the excess neutrons in a neutron-rich nucleus should either increase the fraction of correlated protons or occupy low-momentum states. In either case, the fraction of high-momentum protons should be larger than that of neutrons [13,27,28].

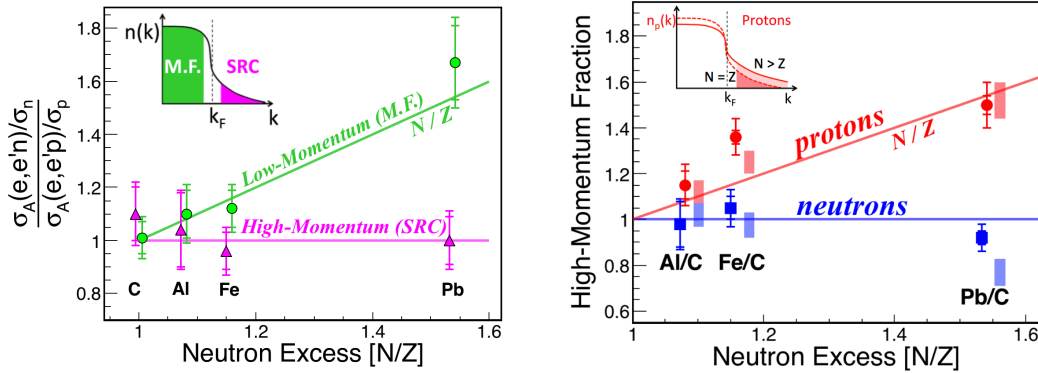


Figure 8: Nucleon knockout studies of heavy nuclei [12]. Left: Extracted ratio of proton to neutron knockout from above and below the nuclear Fermi momentum. Right: Extracted fraction of high-momentum ( $k > k_F$ ) protons and neutrons in nuclei relative to  $^{12}\text{C}$ , compared with SRC model predictions (shaded squares).

In a paper recently published in Nature [12], we reported the first simultaneous measurement of hard QE electron scattering off protons and neutrons (i.e.,  $A(e, e'p)$  and  $A(e, e'n)$  reactions) in  $^{12}\text{C}$ ,  $^{27}\text{Al}$ ,  $^{56}\text{Fe}$ , and  $^{208}\text{Pb}$ . The simultaneous measurement of both proton and neutron knockout allowed a direct comparison of their properties with minimal assumptions. The measurement was made in two different kinematical settings, one corresponding to electron scattering primarily off nucleons from an SRC pair ( $p_{\text{miss}} > k_F$ ), the other from nucleons in the nuclear mean field ( $p_{\text{miss}} < k_F$ ). Using these event samples, the reduced cross-section ratios:  $[A(e, e'n)/\sigma_{en}]/[A(e, e'p)/\sigma_{ep}]$  (i.e., measured cross-sections divided by the known elementary electron-proton,  $\sigma_{ep}$ , and electron-neutron,  $\sigma_{en}$ , cross-sections) were extracted for each kinematical setting. The results shown in Fig. 8 (left) indicate that the  $n/p$  mean-field reduced cross-section ratios grow approximately as  $N/Z$  for all nuclei, as expected from simple nucleon counting. However, the SRC ratios in all nuclei are consistent with unity, consistent with  $np$ -SRC dominance of the high-momentum tail.

To quantify the pairing mechanism leading to constant  $n/p$  ratios for SRC nucleons, we also extracted the relative fraction of high-missing-momentum to low-missing-momentum events in neutron-rich nuclei relative to  $^{12}\text{C}$ , see Fig. 5 (right). This extraction was done separately for protons and neutrons, and shows that the neutron SRC probabilities are independent of the nuclear neutron

excess (i.e. they saturate) while the corresponding proton probabilities grow linearly with  $N/Z$ . This observation indicates that in neutron-rich nuclei, the outer excess neutrons form SRC pairs with protons from the inner ‘core’ of the nucleus.

## 2.5 Reaction Mechanisms Uncertainties in the Interpretation of SRCs

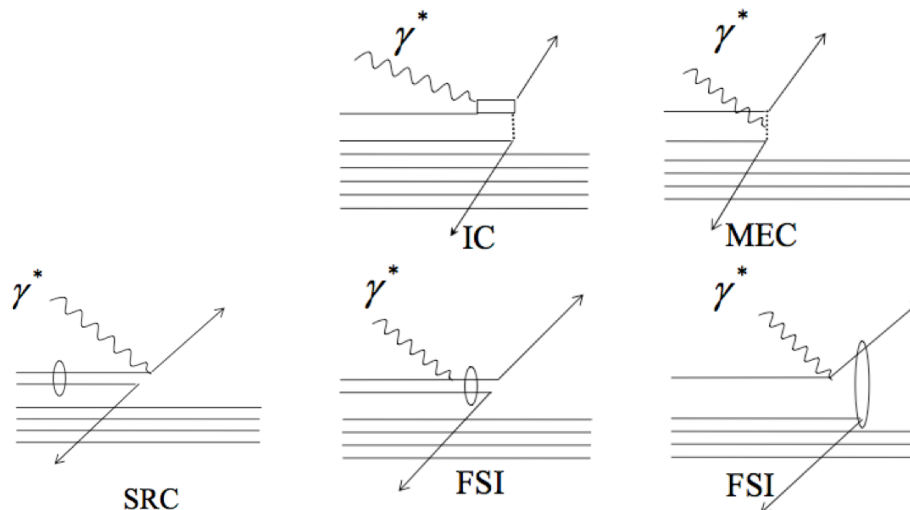


Figure 9: The reaction mechanisms for electron-induced two nucleon knockout. The virtual photon can be absorbed on one nucleon of an SRC pair, leading to the emission of both nucleons (SRC). The virtual photon can excite a nucleon to a  $\Delta$ , which deexcite by exchanging a pion, resulting in the emission of two nucleons (IC). The virtual photon can be absorbed on a pion-in-flight (MEC). The virtual photon can be absorbed on one nucleon of an SRC pair which rescatters from the other nucleon in the pair (FSI (left)). The virtual photon can be absorbed on an uncorrelated nucleon which rescatters from another nucleon (FSI (right)).

The results described above are almost all derived from electron scattering measurements, with only a single proton scattering  $C(p, ppn)$  measurement [23]. Thus, the interpretation of these experimental results relies on an assumed electron interaction mechanism at large momentum transfers. There are a number of different electron-scattering reaction mechanisms that can lead to two-nucleon emission (see Fig. 9). While the experiments described above have been performed at kinematics where many of these effects have been minimized, there are still interpretational uncertainties due to these other possible reaction mechanisms. These reaction mechanisms are not present or are very different for proton scattering.

Photon scattering will also proceed through very different reaction mechanisms. Instead of quasielastic nucleon knockout, the primary photo-induced reaction studied here will be  $\gamma n \rightarrow p\pi^-$ , with a second nucleon (the correlated partner nucleon) emitted backward (see Fig. 10). For this reaction, the IC and MEC reaction mechanisms will be absent or significantly different. In addition, because the correlated partner nucleon will be emitted backwards, the effects of Final State Interactions (FSI) will also be quite different. It is much more difficult to produce backward nucleons than forward ones.

Thus photonuclear measurements of SRCs will provide a crucial reaction mechanism check for SRC studies.

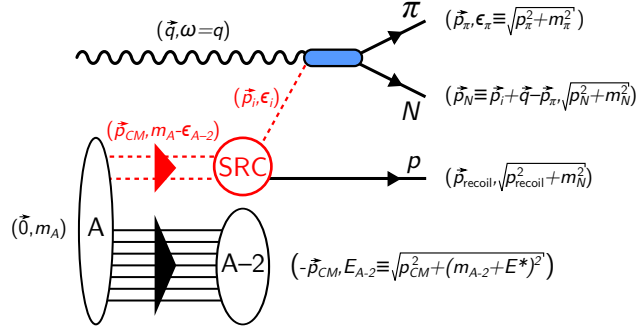


Figure 10: Diagrammatic representation and kinematics of the triple-coincidence  $A(\gamma, \pi N p)$  reaction, one of the main channels of interest for SRC breakup by a real photon beam. As in Fig. 1, dashed red lines represent off-shell particles. Open ovals represent un-detected systems. Solid black lines represent detected particles. The momentum and energy of the particles are also indicated.

### 3 Photonuclear probes of bound nucleon structure

#### 3.1 The EMC Effect and SRCs

The relative abundance of SRC pairs in nuclei can be extracted from measurements of inclusive  $(e, e')$  cross-section ratios for different nuclei at high- $Q^2$ ,  $x_B > 1$  kinematics [6–9, 11, 63–66]. For fixed  $Q^2$ , these cross-section ratios scale as a function of  $x_B$  starting approximately at  $x_B \geq 1.5$ . The height of the scaling plateau is often used to extract the relative number of high-momentum nucleons (i.e. SRC pairs) in the measured nuclei. We refer to these as the ‘SRC scaling coefficients’.

In a recent series of publications [6, 29–31], we and others have shown that the extracted SRC scaling coefficients linearly correlate with the strength of the EMC effect in nuclei from  ${}^3\text{He}$  to  ${}^{197}\text{Au}$ . The latter is the slope of the deviation from unity of the isoscalar DIS cross-section ratio for nuclei relative to deuterium in the range  $0.3 \leq x_B \leq 0.7$ . The EMC effect is commonly interpreted as evidence for modification of the partonic structure function of bound nucleons [6, 60, 61].

The observation of a correlation between the strength of the EMC effect and the SRC scaling coefficients in nuclei generated new interest in the EMC effect (see e.g. CERN Courier cover paper from May 2013; ‘Deep in the nucleus: a puzzle revisited’ [32]) and gave new insight into its possible origin. Several models have been proposed by us and others that attempt to explain the underlying dynamics that drive the EMC effect and its correlation with SRC pair abundances; see a recent review in Ref. [6].

In a data-mining analysis recently published in Nature [11], led by graduate student B. Schmookler and the spokespersons, a high-precision measurement of both the SRC scaling coefficients and the EMC effect was performed for  ${}^{12}\text{C}$ ,  ${}^{27}\text{Al}$ ,  ${}^{56}\text{Fe}$  and  ${}^{208}\text{Pb}$  (see Fig. 11). The new data were used to examine the finer aspects of the EMC-SRC correlation. Specifically, we examined whether the EMC data can indeed be explained by assuming the nuclear structure function can be factorized into a collection of un-modified mean-field nucleons and modified SRC pairs:

$$F_2^A = (Z - n_{\text{SRC}}^A)F_2^p + (N - n_{\text{SRC}}^A)F_2^n + n_{\text{SRC}}^A (F_2^{p*} + F_2^{n*}), \quad (3)$$

where  $n_{\text{SRC}}^A$  is the number of  $np$ -SRC pairs,  $F_2^N(x_B)$  are the free nucleon (proton and neutron) structure functions, and  $F_2^{N*}(x_B)$  are the average modified nucleon structure functions in SRC pairs.  $n_{\text{SRC}}^A$  is taken from experiment (i.e. from  $(e, e')$  scaling ratios at  $x_B > 1.5$ ), and the modified structure function of SRC nucleons,  $F_2^{N*}(x_B)$ , is expected to be universal (i.e., independent of the surrounding nuclear environment).

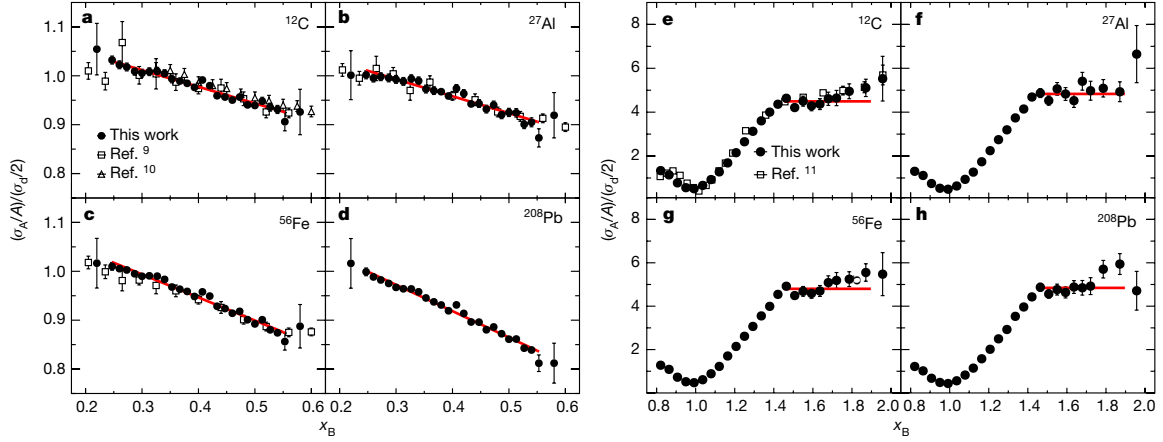


Figure 11: High-precision measurements of the EMC effect (left) and SRC scaling (right) led by the spokespersons [11].

Figure 12 shows the measured structure function ratios of nuclei relative to deuterium (left panel), and the extracted modification function of SRC pairs, using  $\Delta F_2^N = F_2^{N*} - F_2^N$  (right panel). As can be seen, while the nuclear structure functions vary significantly between different nuclei, the extracted SRC pair modification function is universal for all nuclei.

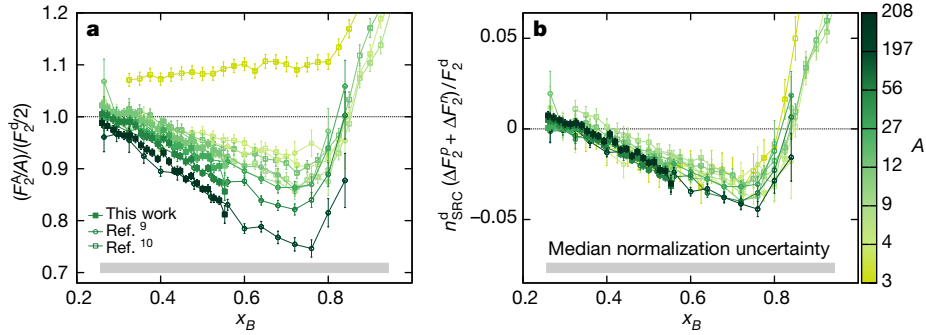


Figure 12: Left: measured structure function ratio for nuclei relative to deuterium (without model-dependent iso-scalar corrections). Right: the extracted universal modification function of nucleons in SRC pairs [11].

### 3.2 Branching ratio modification

To gain further insight to the modification of nucleons bound in SRC pairs, we propose to measure the variation in the Branching Ratios (BRs) for hard photonuclear reactions off free (/quasifree) vs. deeply bound nucleons in the deuteron,  $^4\text{He}$  and  $^{12}\text{C}$ . Changes in the measured BRs, which may depend on the momentum transfer, scattering angle and nuclear transparency, will shed new light on the mechanisms of quark-gluon nucleon structure modification in nuclei. The detailed description of this novel observable follows.

The proton (or neutron) is a complex system that can be described in QCD at any given moment as a superposition of different Fock states:

$$|\text{proton}\rangle = \alpha_{\text{PLC}} |\text{PLC}\rangle + \alpha_{3qg} |3q + g\rangle + \alpha_{3qq\bar{q}} |3qq\bar{q}\rangle + \alpha_{3q\pi} |3q\pi\rangle + \dots \quad (4)$$

Table 1: List of possible exclusive photonuclear reactions off protons and neutrons that are within the detection capabilities of the GlueX spectrometer. Note that neutron reactions are only possible using nuclear targets (deuteron and heavier).

Proton Reactions	Neutron Reactions
$\gamma + p \rightarrow \pi^0 + p$	$\gamma + n \rightarrow \pi^- + p$
$\gamma + p \rightarrow \pi^- + \Delta^{++}$	$\gamma + n \rightarrow \pi^- + \Delta^+$
$\gamma + p \rightarrow \rho^0 + p$	$\gamma + n \rightarrow \rho^- + p$
$\gamma + p \rightarrow K^+ + \Lambda^0$	$\gamma + n \rightarrow K^0 + \Lambda^0$
$\gamma + p \rightarrow K^+ + \Sigma^0$	$\gamma + n \rightarrow K^0 + \Sigma^0$
$\gamma + p \rightarrow \omega + p$	—
$\gamma + p \rightarrow \phi + p$	—

where the different brackets represent states of the proton (or neutron) with the corresponding  $\alpha$  representing the amplitude of each state. By definition all weights must sum to 1. The minimal state of the nucleon includes only the 3 valence quarks and is assumed to be small in size and with a reduced strong interaction. Such a state is referred to as a Point-Like Configuration (PLC). The other states include more complex configuration involving additional gluons, quark-antiquark pairs, pions etc. *These states are all components of the wave function of the nucleon.*

The modified structure of a proton (or neutron) bound in a nucleus can then be represented by a different, decomposition into the same Fock states:

$$|\text{proton}^*\rangle = \alpha_{\text{PLC}}^* |\text{PLC}\rangle + \alpha_{3qg}^* |3q + g\rangle + \alpha_{3qq\bar{q}}^* |3qq\bar{q}\rangle + \alpha_{3q\pi}^* |3q\pi\rangle + \dots \quad (5)$$

where the difference between a free and bound proton is depicted by the difference between the  $\alpha$  and  $\alpha^*$  coefficients in Eqs. 4 and 5. An example of such an effect can be found in the ‘Point Line Configurations Suppression’ model of Frankfurt and Strikman [67] or the ‘Blob-Like Configurations Enhancement’ model of Frank, Jennings, and Miller [68] that propose a possible explanation to the EMC effect in which the PLC part of the bound nucleon is different than in a free one.

We stress that the Fock space description of bound nucleons is somewhat more complex as nucleons bound in nuclei span various states: e.g. mean-field vs. SRC nucleons, high vs. low local density etc., allowing the  $\alpha^*$  coefficients to possibly depend on the detailed nuclear state of the bound nucleon. For example, in the PLC suppression model [67],  $|\alpha_{\text{PLC}}^*/\alpha_{\text{PLC}}|^2 - 1$  is proportional to the nucleon off-shellness (approximately to the square of the nucleon momentum) with much smaller modification for configurations close to the average ones. Hence one expects maximal bound nucleon modification in the processes dominated by scattering from small size configurations.

We expect that different Fock states will absorb high-energy photons differently and lead to different branching ratios (BR) for various final states (e.g.,  $\gamma p \rightarrow \pi^- \Delta^{++}; \rho^0 p$ ). We propose to use the unique capability of GlueX to measure simultaneously the BRs of many decay channels of an excited nucleon following the absorption of a real photon at high momentum transfer (large  $t$ ). By measuring these BR for nucleons in a range of nuclei from deuterium through lead we will be able to see differences in the Fock state decomposition, and hence the structure, of bound and free nucleons.

For a free proton GlueX will measure the branching ratio (BR) for many reactions, including  $\gamma p \rightarrow \pi^- \Delta^{++}, \rho^0 p, K^+ \Lambda, K^+ \Sigma^0$ , and others. By measuring these reactions, and the neutron equivalents (listed in Table 1), on deuteron and nuclear targets, we can extract the BRs for scattering off free (/quasi-free) vs. deeply bound nucleons. As each reaction is sensitive to a different combination of Fock states, modifying their contribution to the bound proton will modify their BRs.

Current theoretical models do not allow us either to predict the exact change in BRs as a function

of the bound nucleon structure, or to translate the observable BRs to the modified  $\alpha^*$  coefficients. However, this is a novel observable that allows us to observe or exclude deviations, and to study their dependence on the nucleon momentum and ‘hardness’ of the reaction. Any such observation will therefore serve as clear and direct evidence for changes in bound nucleon structure.

On average, differences between a bound and a free nucleon are expected to be small. However, we propose to select specific kinematics, focusing on deeply bound nucleons, that could enhance the effect: e.g., selecting hard process with large  $s$ ,  $t$ , and  $u$  is expected to emphasize the contribution of the PLC component. Alternatively, detecting the decay products along with a high-momentum recoil nucleon (which favors scattering from a nucleon from an SRC pair) should also significantly amplify the medium effect to the level observed for the EMC effect at  $x_B \sim 0.5$ – $0.6$  that is modification on the scale of 20%. The high-momentum recoil nucleons can best be studied with a deuteron target.

In the case of nuclear targets, the measured BRs are not at the photon absorption point but rather following hadron attenuation in the nucleus, which may be different for each channel. To extract the BR at the hard vertex of the quasi-free scattering we need to correct for hadron attenuation in the nucleus. We propose to do that by measuring the process on deuterium, helium and carbon. This will yield, as a byproduct, an interesting study of photon and Color Transparency (CT), as well as measure pattern of interaction with media of different mesons. See separate discussion on CT below.

## 4 CT at High Energies

In addition to SRCs and bound nucleon structure, the data to be collected in this experiment will be used to study hadron color transparency (CT). At high energies, the phenomena of CT arises from the fact that exclusive processes on a nucleus at high momentum-transfer preferentially select the color singlet, small transverse size configuration, which then moves with high momentum through the nucleus. The interactions between the small transverse size configuration and other nucleons are strongly suppressed because the gluon emission amplitudes arising from different quarks cancel. This suppression of the interactions is one of the essential ingredients needed to account for Bjorken scaling in deep-inelastic scattering at small  $x_B$  [45].

CT at high energies was directly observed in the diffractive dissociation of 500 GeV/ $c$  pions into dijets when coherently scattering from carbon and platinum targets. The per-nucleon cross-section for dijet production is parametrized as  $s = s_0 A^a$ , and the experiment found  $a = 1.61 \pm 0.08$  [69], consistent with CT predictions of  $a = 1.54$  [70]. These results confirm the predicted strong increase of the cross-section with  $A$ , and the dependence of the cross-section on the transverse momentum of each jet with respect to the beam axis ( $k_t$ ) indicates the preferential selection of the small transverse size configurations in the projectile. Such experiments have unambiguously established the presence of small-size  $q\bar{q}$  Fock components in light mesons and show that at transverse separations,  $d \sim 0.3$  fm, pQCD reasonably describes small  $q\bar{q}$ -dipole-nucleon interactions. Thus, color transparency is well established at high energies and low  $x_B$ . However, these high-energy experiments do not provide any information about the appropriate energy regime for the onset of CT.

At intermediate energies, in addition to the preferential selection of the small-size configuration, the expansion of the interacting small-size configuration is also very important. At these energies, the expansion distance scales are not large enough for the small-size configuration to escape without interaction which, suppresses the color transparency effect [71–74]. The interplay between the selection of the small transverse size and its subsequent expansion determine the scale of the momentum and energy transfers required for the onset of CT. As mentioned, a major difference between photo-induced and electron-induced reactions is that, in the former, much greater energy is transferred relative to momentum, which can help disentangle the roles of freezing and squeezing.

The first attempt to measure the onset of CT at intermediate energies used the large-angle  $A(p, 2p)$  reaction at the Brookhaven National Lab (BNL) [75–78]. In these experiments, large-angle

$pp$  and quasielastic ( $p, 2p$ ) scattering were simultaneously measured in hydrogen and several nuclear targets, at incident proton momenta of 6–12 GeV/ $c$ . The nuclear transparency was extracted from the ratio of the quasielastic cross-section from a nuclear target to the free  $pp$  elastic cross-section. The transparency was found to increase as predicted by CT, but only between 6–9.5 GeV/ $c$ ; the transparency was found to decrease between 9.5 and 14.4 GeV/ $c$ . This decrease cannot be explained by models incorporating CT effects alone. Though not fully understood to date, this behavior is commonly attributed to a lack of understanding of the fundamental two-body reactions, which limits one’s ability to relate the  $s$ ,  $t$  scales for the onset of squeezing in different reactions. This situation raises doubts about our ability to study CT effects using such proton-induced QE scattering reactions.

In contrast to hadronic probes, weaker electromagnetic probes sample the complete nuclear volume. The fundamental electron-proton scattering cross-section is smoothly varying and is accurately known over a wide kinematic range. Detailed knowledge of the nucleon energy and momentum distributions inside a variety of nuclei have been extracted from extensive measurements in low-energy electron scattering experiments. Therefore, the ( $e, e'p$ ) reaction is simpler to understand than the ( $p, 2p$ ) reaction, an advantage immediately recognized following the BNL ( $p, 2p$ ) experiments. A number of  $A(e, e'p)$  experiments have been carried out over the years, first at SLAC [79, 80] and later at JLab [81, 82] for a range of light and heavy nuclei. In high  $Q^2$  quasielastic ( $e, e'p$ ) scattering from nuclei, the electron scatters preferably from a single proton, which need not be stationary due to Fermi motion [83]. In the plane wave impulse approximation (PWIA), the proton is ejected without final state interactions with the residual  $A - 1$  nucleons. The measured  $A(e, e'p)$  cross-section would be reduced compared to the PWIA prediction in the presence of final state interactions, where the proton can scatter both elastically and inelastically from the surrounding nucleons as it exits the nucleus. The deviations from the simple PWIA expectation is used as a measure of the nuclear transparency. In the limit of complete color transparency, the final state interactions would vanish and the nuclear transparency would approach unity. In the conventional nuclear physics picture, one expects the nuclear transparency to show the same energy dependence as the energy dependence of the  $NN$  cross-section. Other effects such as short-range correlations and the density dependence of the  $NN$  cross-section will affect the absolute magnitude of the nuclear transparency but have little influence on the energy- (or  $Q^2$ -) dependence of the transparency. Thus, the onset of CT is expected to be manifested as a rise in the nuclear transparency as a function of increasing  $Q^2$ .

The existing world data rule out any onset of CT effects larger than 7% over the  $Q^2$  range of 2.0–8.1 (GeV/ $c$ )<sup>2</sup> with a confidence level of at least 90%. As mentioned earlier, the onset of CT depends both on momentum and energy transfers, which affect the squeezing and freezing respectively. Since  $A(e, e'p)$  scattering measurements are carried out at  $x_B = 1$  kinematics, they are characterized by lower energy transfers as compared to the momentum transfer (e.g. 4.2 GeV for  $Q^2 = 8$  GeV<sup>2</sup>). Existing data seem to suggest that a  $Q^2$  of 8 (GeV/ $c$ )<sup>2</sup> with 4.2 GeV energy transfer is not enough to overcome the expansion of the small transverse size objects selected in the hard  $ep$  scattering process (i.e. freezing requirements are not met). A recent Hall C 12 GeV experiment, currently under analysis, will extend these studies to  $Q^2 \sim 16$  GeV<sup>2</sup> [84]. Although, no unambiguous evidence for CT has been observed so far for nucleons from either  $A(e, e'p)$  or  $A(p, 2p)$  reactions, it is expected to be more probable to reach the CT regime at low energy for the interaction/production of mesons than for baryons, since only two quarks must come close together and a since a quark-antiquark pair is more likely to form a small size object [85]. Indeed, pion production measurements at JLab reported evidence for the onset of CT [86] in the process  $e + A \rightarrow e + p + A^*$ . The pion-nuclear transparency was calculated as the ratio of pion electroproduction cross-section from the nuclear target to that from the deuteron. As proposed here, the use of the deuteron instead of the proton helped reduce the uncertainty due to the unknown elementary pion electroproduction cross-section off a free neutron and to uncertainties in the Fermi smearing corrections. The measured pion nuclear transparency shows a steady rise with increasing pion momentum for the  $A > 2$  targets, and this rise in nuclear transparency versus  $p_\pi$  is consistent with the rise in transparency predicted by various CT

calculations [87–89]. Although, all the calculations use an effective interaction based on the quantum diffusion model [71] to incorporate the CT effect, the underlying conventional nuclear physics is calculated very differently. The results of the pion electroproduction experiment demonstrate that both the energy and  $A$  dependence of the nuclear transparency show a significant deviation from the expectations of conventional nuclear physics and are consistent with calculations that include CT. The results indicate that the energy scale for the onset of CT in mesons is  $\sim 1$  GeV.

Electroproduction of vector mesons from nuclei is another excellent tool to investigate the formation and propagation of quark-antiquark ( $q\bar{q}$ ) pairs under well-controlled kinematical conditions. Soon after the observation of the onset of CT in pion electroproduction, results from a study of  $\rho$ -meson production from nuclei at JLab also indicated an early onset of CT in mesons [90]. Previous  $\rho^0$  production experiments had shown that nuclear transparency also depends on the coherence length,  $l_c$ , which is the length scale over which the  $q\bar{q}$  states of mass  $M_{q\bar{q}}$  can propagate. Therefore, to unambiguously identify the CT signal, one should keep  $l_c$  fixed while measuring the  $Q^2$  dependence of the nuclear transparency. The CLAS collaboration at JLab measured the nuclear transparency for incoherent exclusive  $\rho^0$  electroproduction off carbon and iron relative to deuterium [90] using a 5 GeV electron beam. An increase of the transparency with  $Q^2$  for both C and Fe, was observed indicating the onset of CT phenomenon. The rise in transparency was found to be consistent with predictions of CT by models [91,92] which had successfully described the increase in transparency for pion electroproduction. Therefore, the  $\pi$  and  $\rho$  electroproduction data also demonstrate an onset of CT in the few GeV energy range as shown in Figure 13. Both of these experiments will be extended to higher energies in future 12 GeV experiments [84,93].

In the case of large momentum transfer exclusive photoinduced reactions, while the predicted effects are larger (Fig. ??) they were not studied in much detail. JLab experiment E94-104 searched for CT using the reaction  $\gamma + n \rightarrow \pi^- + p$  [94]. The experiment used an untagged mixed electron and photon bremsstrahlung beam incident on a  $^4\text{He}$  target and the Hall-A high-resolution spectrometers to measure  $\pi^-$  and  $p$  produced in the reaction. The momentum transfer was reconstructed assuming scattering off a mean-field neutron in  $^4\text{He}$  leaving the residual system in the ground state of  $^3\text{He}$ . Nuclear transparency was measured as a ratio of the pion photoproduction cross-section from  $^4\text{He}$  to that of  $^2\text{H}$ . Figure 14 shows the extracted transparency as a function of the momentum transfer,  $|t|$ , for center-of-mass scattering angles of  $70^\circ$  and  $90^\circ$ . The results were compared to Glauber calculations with and without CT effects. As can be seen, the measurement did not have the required statistical and systematical accuracy to discriminate between the two calculations over the measured  $|t|$  range. We propose, using the advantages of the GlueX spectrometer and the upgraded CEBAF 12 GeV electron beam, to add many more reaction channels, extend the measured  $|t|$  range up to 10–12 GeV<sup>2</sup>, and add heavier nuclei. While we will keep comparable uncertainties, for heavier nuclei and larger momentum transfers the expected effects are considerably larger, which significantly increases the discovery potential.

It should be pointed out that the rate of expansion/contraction of configurations involved in the interaction with nucleons is the same for the different reactions. Hence, in light of the successful description of CT for mesons, reliable estimate of space-time evolution effects were performed for other reactions with the conclusion that in the proposed kinematics for GlueX, CT is not washed out by the expansion/contraction effects due to the high photon energies used in the experiment.

## 5 The Proposed Measurement

### 5.1 Kinematics

The kinematical distributions and expected event rates were simulated for the pion-proton photoproduction reaction off a neutron bound in a nucleus,  $A(\gamma, \pi^- p)$ , using a dedicated Monte-Carlo event generator. In this section, we present the simulation method and show the resulting kinematical distributions.

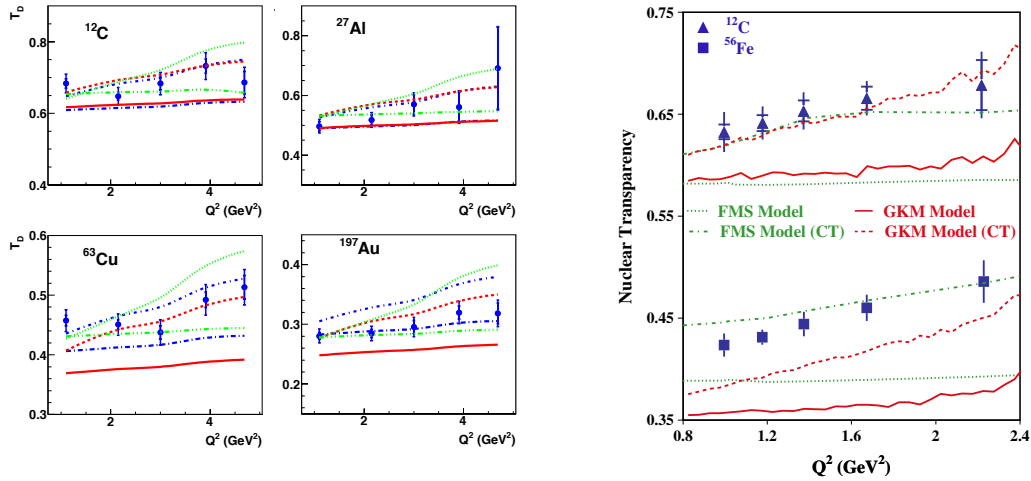


Figure 13: The two JLab experiments which show conclusive evidence for the onset of CT in meson electroproduction at intermediate energies. **(left panel)** Nuclear transparency vs  $Q^2$  for  $^{12}\text{C}$ ,  $^{27}\text{Al}$ ,  $^{63}\text{Cu}$  and  $^{197}\text{Au}$  in the  $(e, e'\pi^+)$  reaction. The inner error bars are the statistical uncertainties and the outer error bars are the statistical and point-to-point systematic uncertainties added in quadrature. The solid circles (blue) are the high- $\epsilon$  (virtual photon polarization) points, while the solid squares (red) are the low- $\epsilon$  points. The dashed and solid lines (red) are Glauber calculations from [87], with and without CT, respectively. Similarly, the dot-short dash and dot-long dash lines (blue) are Glauber calculations with and without CT from [88]. The dotted and dot-dot-dashed lines (green) are microscopic+ BUU transport calculations from [89], with and without CT, respectively. **(right panel)** Nuclear transparency as a function of  $Q^2$  in the  $(e, e'\rho^0)$  reaction. The curves are predictions of the FMS [91] (red) and GKM [92] (green) models with (dashed-dotted and dashed curves, respectively) and without (dotted and solid curves, respectively) CT. Both models include the pion absorption effect when the  $\rho^0$  meson decays inside the nucleus. The inner error bars are the statistical uncertainties and the outer ones are the statistical and the point-to-point systematic uncertainties added in quadrature.

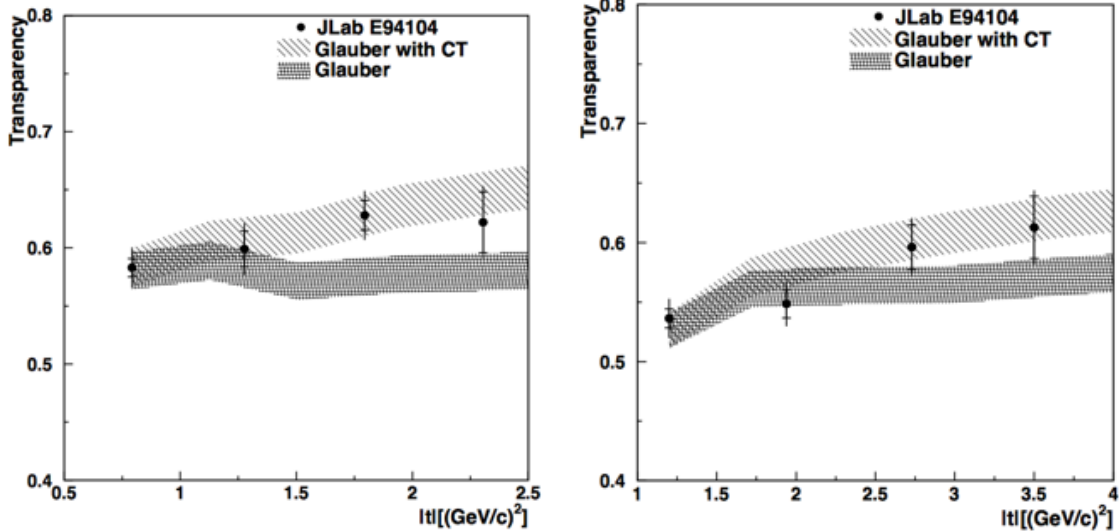


Figure 14: The measured transparency for the reaction  ${}^4\text{He}(\gamma, \pi^- p)$  for two c.m. scattering angles ( $70^\circ$ -right,  $90^\circ$ -left). The measurements are compared to Glauber calculations with and without CT. See Ref. [91] for details.

The simulation uses an incoming photon with energy sampled from the tagged photon spectra obtained from the standard GlueX simulation software (Fig. 15). The momentum distribution of the nucleons in the nucleus has two components: a mean-field region that spans low momentum (up to  $k_F$ ) and account for 80% of the nucleons and an SRC region that spans high momentum (from  $k_F$  and up) and account for 20% of the nucleons. The SRC-pairs are modeled using a three-dimensional Gaussian center of mass momentum distribution with width (sigma) of  $140 \text{ MeV}/c$  [15, 16, 23, 53, 54] In the case of the deuteron, the AV18 momentum distribution was used.

The cross-section for the  $\gamma + n \rightarrow \pi^- + p$  reaction was calculated based on the experimental data for  $90^\circ$  scattering in the c.m. with  $s > 6.25 \text{ GeV}^2$  assuming factorization of the  $s$  and c.m. angle dependence, i.e.,  $\frac{d\sigma}{dt}|_{\theta_{c.m.}} = (C \times s^{-7}) \times f(\theta_{c.m.})$ , where  $C$  is a free fit parameter and  $f$  was extracted from the SLAC data assuming  $f(90^\circ) = 1$  [95], see Fig. 16.

The scattering was performed in the c.m. frame of the bound nucleon and gamma beam for scattering angles of  $40^\circ$ – $140^\circ$ . Hard reaction kinematics were enforced by requiring  $|t, u| > 2 \text{ GeV}^2$ . We note that the rate for lower momentum transfers is very high and within the GlueX acceptance. Figures 17 and 18 show the kinematical distributions for the final state particles respectively for interactions of the gamma with a mean-field nucleon and an SRC nucleon. For the case of SRC pair breakup, the distribution of the correlated recoil proton is shown in Fig. 19. As mentioned, the backward peak of the recoil proton is due to the  $s^{-7}$  weighting of the cross-section that prefers interactions with forward going nucleons which, in the case of SRCs, enforce the recoil nucleon to be emitted in a backward direction. We note that the resulting kinematical distributions are not very different from those obtained for scattering off stationary nucleons, which is what GlueX was designed to do.

The simulation results were compared to a simple, back-of-the-envelope calculation for the reaction cross-section. This calculation is explained in Appendix A. The back-of-the-envelope result is within 20% of the simulation, giving us confidence in the validity of our simulation.

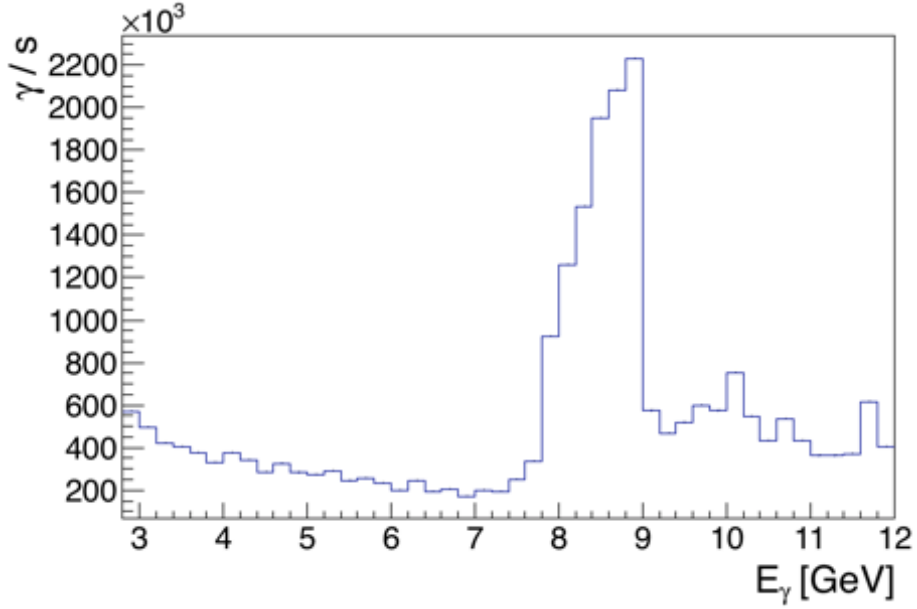


Figure 15: The energy distribution for the incoming photon beam hitting the GlueX target assuming a 5 mm diameter collimator. The distribution is normalized to a flux of  $2.5 \times 10^7$  photons/s in the beam energy range  $7.5 \text{ GeV} < E_{\text{beam}} < 11.7 \text{ GeV}$ .

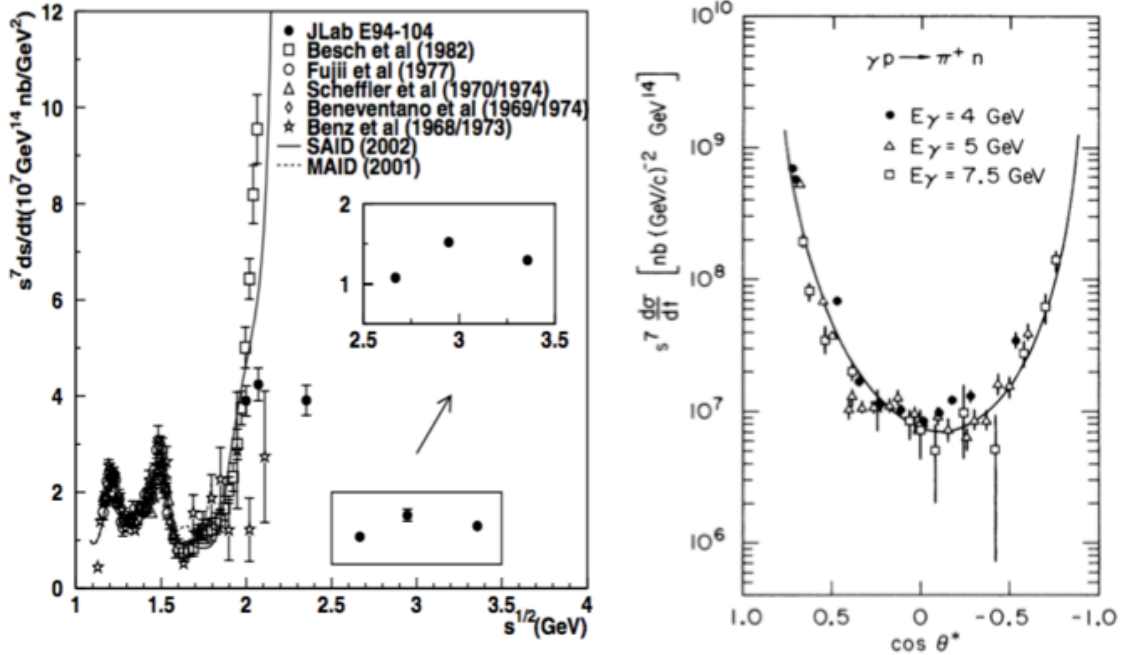


Figure 16: The  $s$  dependence of the photoneuclear cross-section at  $90^\circ$  in the c.m. (left) and its dependence on the c.m. angle (right). We extract the cross-section by fitting the  $s$  dependence at high- $s$ , after the low- $s$  oscillations appear to be over. Figures were adapted from [95].

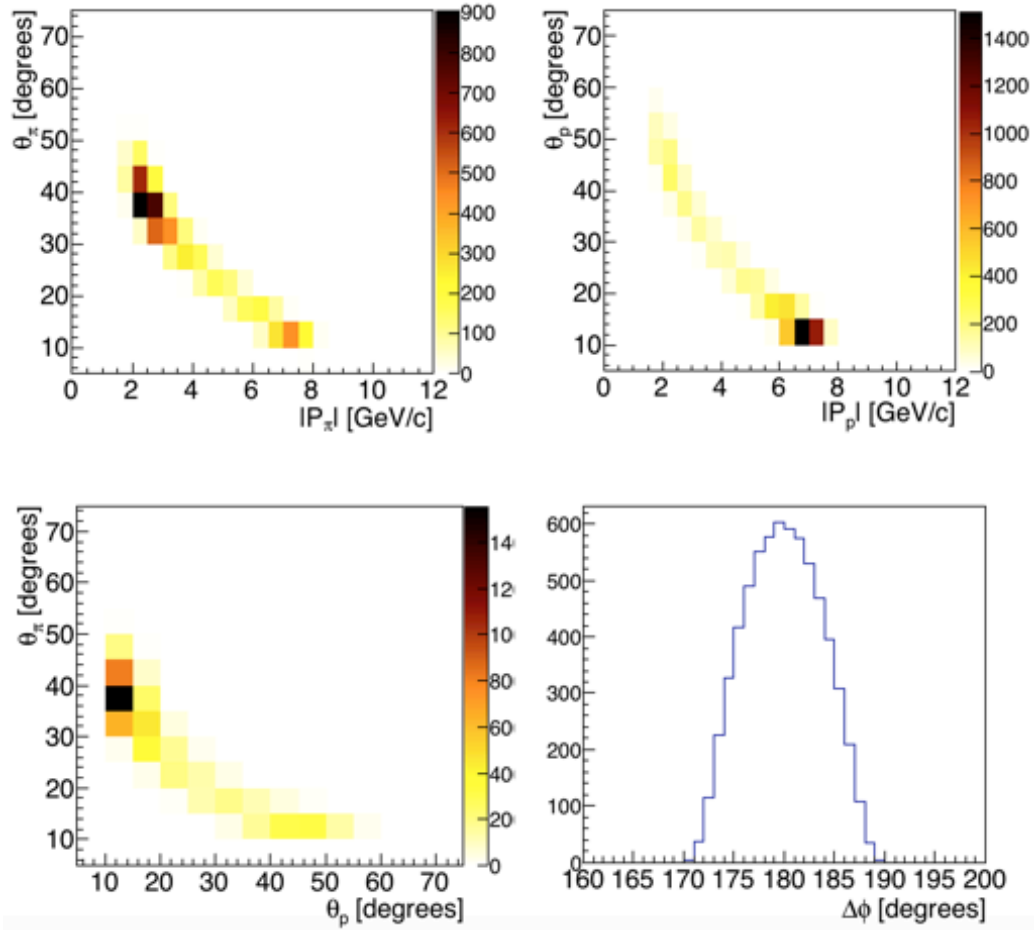


Figure 17: Kinematical distributions for the final state particles of the  $\gamma + n \rightarrow \pi^- + p$  reaction for the MF regime ( $P_{\text{miss}} < 0.25 \text{ GeV}/c$ ).

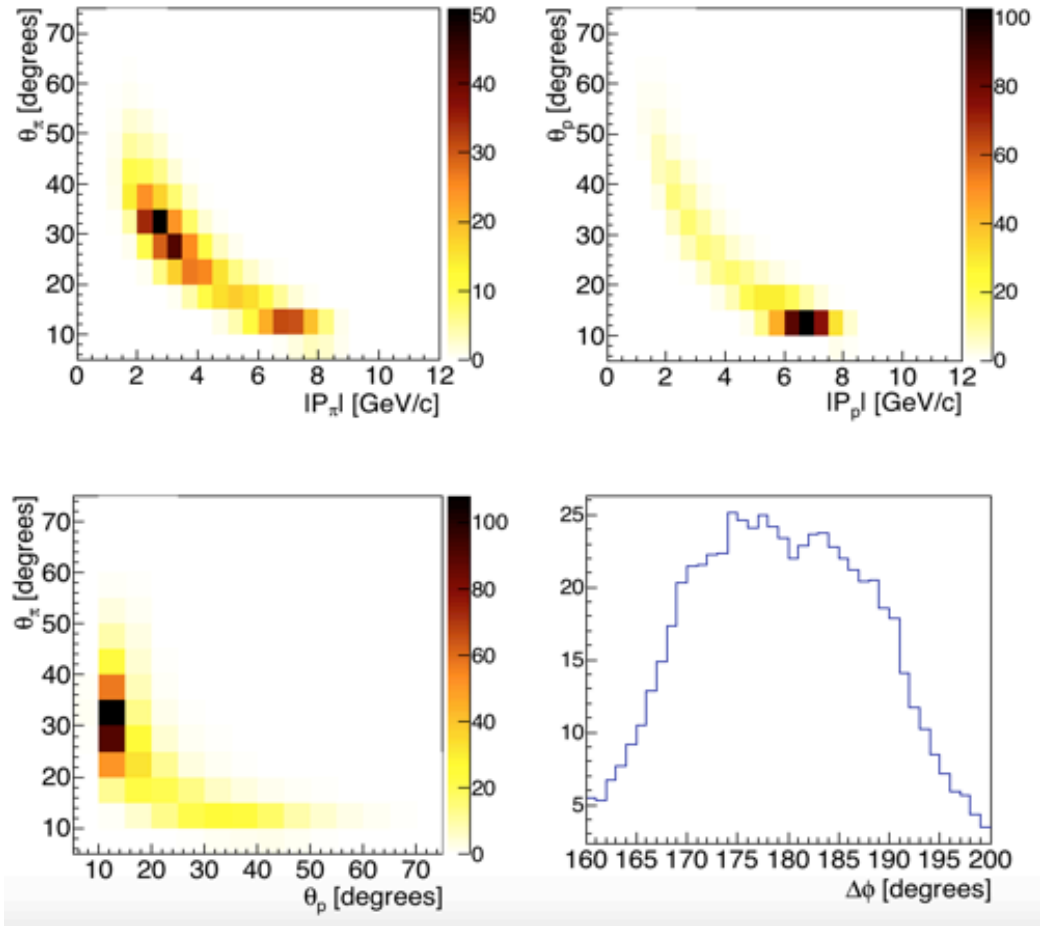


Figure 18: Same as Fig. 17 for the SRC regime ( $P_{\text{miss}} > 0.25$  GeV/c and  $q_{\text{recoil}} < 160^\circ$ ).

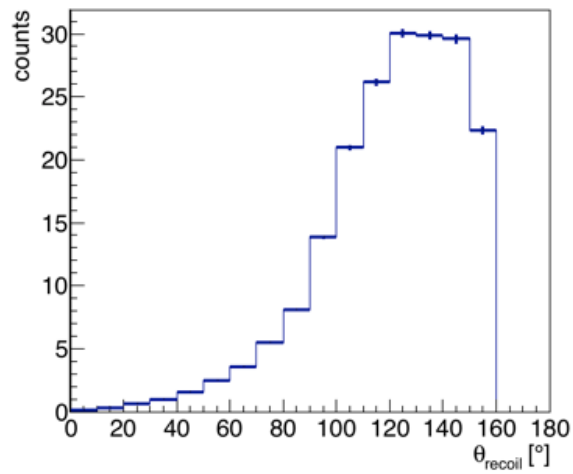


Figure 19: The angular distribution of the recoil nucleus when scattering off an SRC pair in the nucleus.

## 5.2 Optimization of the Tagged Gamma Energy Range

The Hall-D beam allows for a broad distribution of tagged photons on the target (Fig. 15). Due to the coincidental rate limitation of the Hall-D tagger we cannot consider the full gamma spectrum and should focus on a given energy range. Fig. 20 shows the correlation of  $|t|$  and the beam-energy. As we are largely interested in large  $|t|$  reactions, we choose to focus the tagger at the coherent peak, with gamma energies of  $8 \text{ GeV} < E_{\text{beam}} < 9 \text{ GeV}$ .

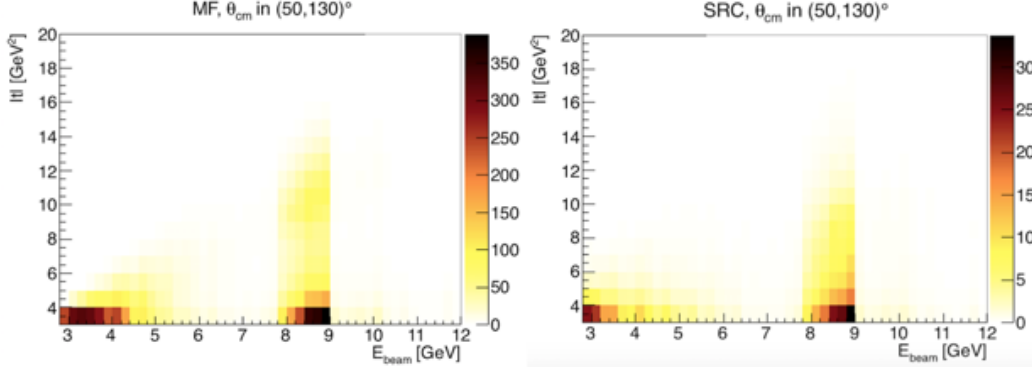


Figure 20: The momentum transfer  $|t|$  as a function of the photon beam energies for two regimes of event selection: MF on the left and SRC on the right. The center of mass angle is in the range between  $50^\circ$  and  $130^\circ$ .

The number of photons in the coherent peak is regulated by the size of the collimator: a wider collimator ensures more coherent photons to hit the target. A collimator diameter of 5 mm was found to be optimal, as it allows measuring all the coherent photons with minimal ‘background’ from low energy photons. Smaller collimator will reduce the high-energy gamma flux and larger collimator will increase the low energy background (leading to larger EM and neutron backgrounds) without improving the high-energy gamma flux.

The factors limiting the beam luminosity are the coincidental rate in the tagger and the electromagnetic background level in the GlueX spectrometer. The tagger coincidental rate for a photon flux on the target of  $2 \times 10^7$  photons/s and RF time of 4 ns is expected to be about 18%.

To be conservative, the rate calculations presented below (and kinematical distribution presented above) are done for photon beam energies in the  $8 \text{ GeV} < E_{\text{beam}} < 9 \text{ GeV}$  range alone.

## 5.3 Final State Particle Detection

The efficiencies for the reconstruction of final state particles (i.e. meson-baryon pair and, in the case of SRC breakup, also the recoil proton) were simulated using the Geant-based GlueX simulation chain for the event generator described in the previous section. Fig. 21 shows the simulated detection efficiency for each particle separately. The average efficiency for the simultaneous reconstruction of the proton and a pion was found to equal 64%.

Based on the current GlueX data reconstruction efficiencies, we expect that more complex final states will have varying detection efficiencies reaching down to 30% for rho mesons. The total detection efficiency for the reaction  $\gamma + n \rightarrow \rho^- + p$  is therefore assumed to be  $0.9 \times 0.3 = 27\%$ .

In the case of SRC pair breakup, one should also take into account the detection efficiency of the recoil proton in the backward hemisphere. Figure 21 also shows the simulated detection efficiency of the recoil proton for the case of SRC pair breakup. Fig. 22 shows the detailed acceptance and detection efficiency for recoiling protons for 3 different vertex positions—at the center and two ends of the 30 cm long hydrogen target. As can be seen, the detection efficiency is very high up to  $140^\circ$  in

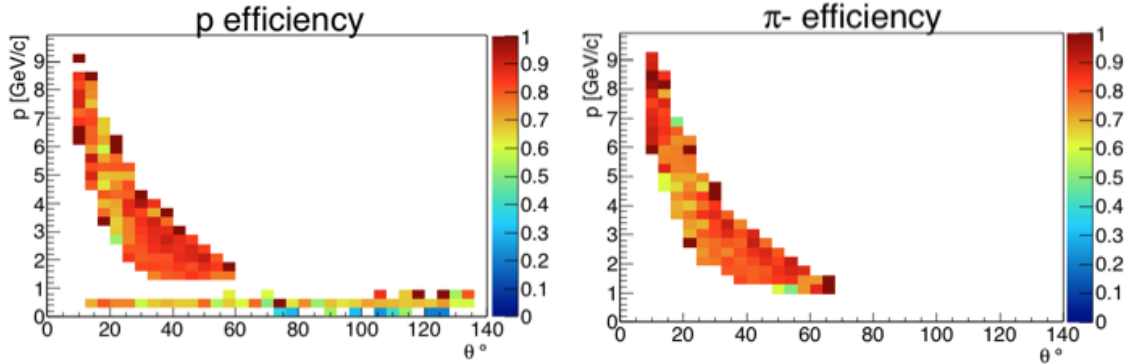


Figure 21: The reconstruction efficiency for the charged tracks coming from the reaction  $\gamma n \rightarrow \pi^- p$ . On the left panel the low momentum band is due to recoil protons from SRC pair breakup.

the lab and can extend up to  $160^\circ$  when the target is placed downstream. Fig. 23 shows the vertex reconstruction resolution, showing we can separate solid target foils with a distance of  $\sim 1$  cm which is more than enough to separate different foils in the case of  $^{12}\text{C}$ .

## 5.4 Expected Rates

The rate calculations were done for the  $\gamma + n \rightarrow \pi^- + p$  and  $\gamma + n \rightarrow \rho^- + p$  reactions, using the simulation presented in section 5.1. We choose these two reactions as they have the smallest and largest cross-sections respectively, of the reactions listed in table 1 which makes them a good representative of the various expected rates.

We assume a total of 30 beam days with a photon flux of  $2 \times 10^7 \text{ s}^{-1}$  (compared to the nominal GlueX photon flux of  $10^8$  photons/s) and four targets: D,  $^4\text{He}$ , and  $^{12}\text{C}$ . Based on the acceptance simulations presented above, we assume 80% detection efficiency for each of the leading baryon and meson and 65% for the recoil nucleon. We assume the nominal nuclear attenuation effect reduces the total cross-section as  $A^{-1/3}$ . Table 2 lists the parameters for the chosen targets. The factors limiting the event rates are the following:

- GlueX detector capabilities (maximum possible gamma flux on target)
- Electromagnetic background in the GlueX spectrometer
- Tagger coincidental rate
- Neutron background

Presently, GlueX is operating with a 30 cm long liquid hydrogen (LH) target (3.4% radiation length,  $X_0$ ). For the nominal beam flux on the target of  $10^8$  photons/s the electromagnetic background is reaching its upper limit. In order to comply with the electromagnetic background limits, we assume the carbon target thickness to be 7%  $X_0$  (note that unlike for hydrogen, for nuclei there are 2 nucleons for each electron in the target. Therefore, for EM background estimations, 7%  $X_0$  on nuclei is equivalent to 3.5%  $X_0$  on hydrogen). The radiation lengths for liquid hydrogen, deuterium, and helium are similar. The use of nuclear targets will increase the slow neutron background that can induce some damage to GlueX detector components such as the SiPMs. Table 2 shows an estimate of the neutron background, done in collaboration with Hall D staff, based on JLAB-TN-11-005. GlueX was designed to handle one year of LH running with a photon flux of  $10^8$  photons/s. While the proposed gamma flux for this measurement is smaller by a factor of 5, detailed estimations by

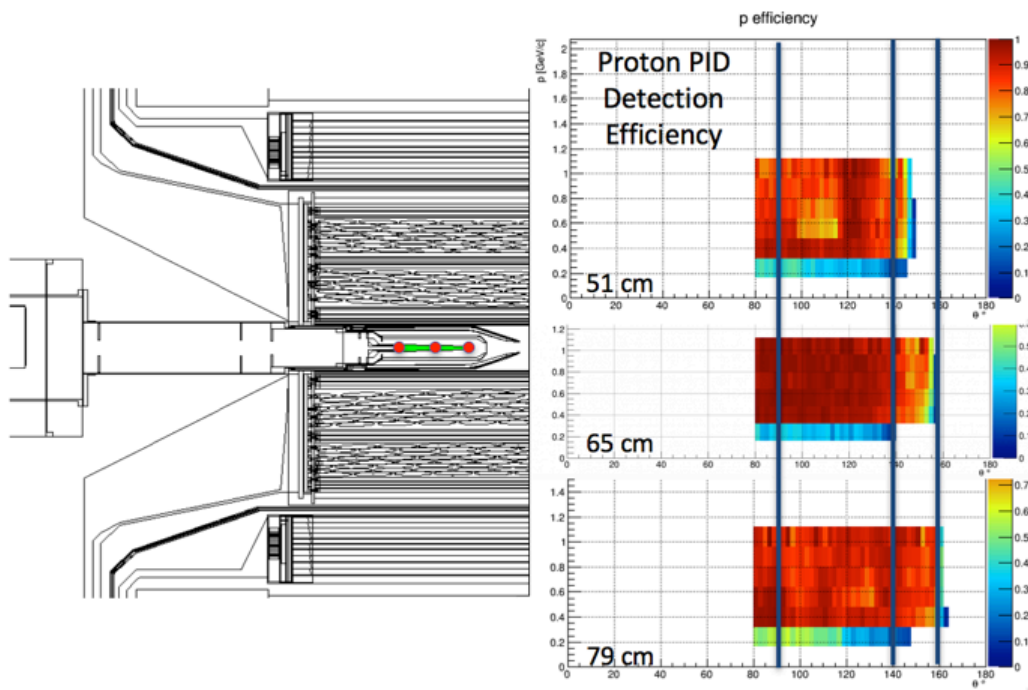


Figure 22: The detection efficiency for recoiling protons in GlueX as a function of the recoil angle and momentum for 3 different vertex locations.

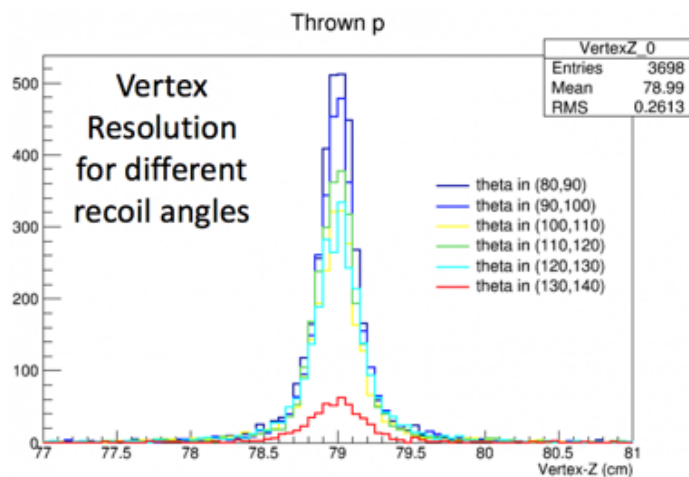


Figure 23: The vertex reconstruction resolution for recoiling protons at various recoil angles.

Table 2: Parameters for the proposed targets. The current GlueX liquid hydrogen target (LH) is shown for comparison. (\*) The neutron flux for the LH target is taken under assumption of the nominal flux of  $10^8$  photons/s in the coherent peak.

Target	Thickness [cm] / % $X_0$	Atoms/cm <sup>2</sup> for the given target thickness	EM bkg. rel. to GlueX	Neutron bkg. rel. to GlueX
D	30 / 4.1	$1.51 \times 10^{24}$	0.5	1.3
<sup>4</sup> He	30 / 4	$5.68 \times 10^{23}$	0.5	1
<sup>12</sup> C	1.9 / 7	$1.45 \times 10^{23}$	1	0.8
LH	30 / 3.4	$1.28 \times 10^{24}$	1	1*

Table 3: Event rates estimation. See text for details.

Target	$\gamma + n \rightarrow \pi^- p$		$\gamma + n \rightarrow \rho^- p$		PAC Days
	MF	SRC	MF	SRC	
D	13,600	750	57,000	3,000	5
<sup>4</sup> He	16,000	840	68,000	3,500	10
<sup>12</sup> C	8,900	2,800	37,000	11,000	12
Calibration, commissioning, and overhead:					3
<b>Total PAC Days:</b>					<b>30</b>

the Radcon group, backed with relevant measurements, show that replacing the LH target with <sup>4</sup>He will increase the neutron background by a factor of 4-5 (depending on the exact location). This implies that the neutron background for <sup>4</sup>He target in our running conditions will be similar to the GlueX design specifications. The estimated neutron backgrounds for all targets are shown in table 2, and are calculated from the Radcon <sup>4</sup>He estimate and their reported  $A$ -dependence. For reference, the table includes the GlueX LH target under nominal running conditions, i.e.  $10^8$  photons/s. The background rates for the other targets take into account the five-fold reduced gamma flux for the proposed experiment. While this background estimation procedure takes into account the main differences coming from nuclear targets relative to LH, the deuteron backgrounds could be somewhat higher. Given the very short deuteron beam time (table 3) this should not be an issue with regard to integrated damage.

Table 3 lists the expected events rate and beam time for each target for  $|t, u| > 2 \text{ GeV}^2$  for mean-field and SRC events separately. For Deuterium, as we use the AV18 distribution, the distinction is based on the initial momentum of the nucleon that the gamma interacted with (above or below 250 MeV/c). Figure 24 shows the expected count rate of various  $|t|$  bins for Deuterium and <sup>12</sup>C for mean-field events. The statistics for  $|t| < 2 \text{ (GeV/c)}^2$  is rich, allowing to map the transition between different transparency regimes. Other nuclei have the same  $|t|$  dependence and the expected count rate per bin can be scaled based on the total number of events listed in Table 3. We have chosen to distribute the beam time between the different targets so as to obtain comparable discriminating power for transparency studies and scaling of SRC pairs; the larger nuclei have larger predicted effects and therefore fewer statistics are needed to observe them at similar levels of significance.

Fig. 25 shows the expected results for the color transparency for the  $\gamma + n \rightarrow \pi^- + p$  reaction. Other reactions from table 1 will have comparable or better discriminating power. We note that by taking ratios for nuclei relative to deuterium we minimize many of the theoretical systematical

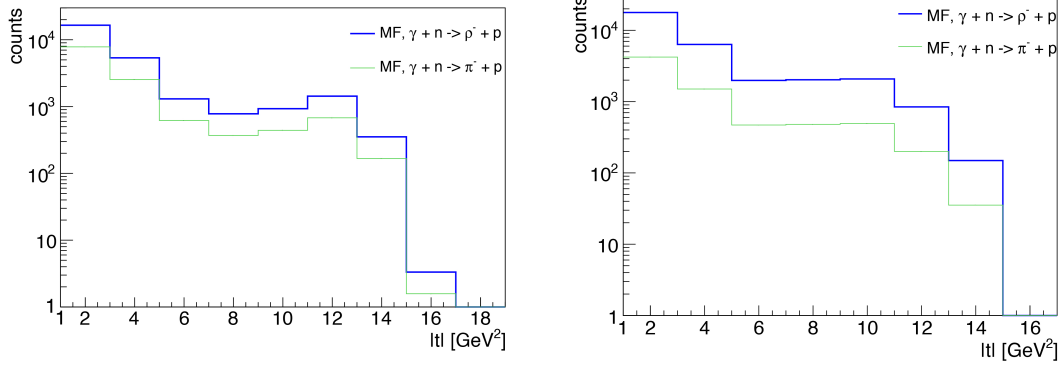


Figure 24: The expected count rate for 10 days running as a function of  $|t|$  for Deuterium (left) and  $^{12}\text{C}$  (right) targets in mean-field kinematics for two different reactions.

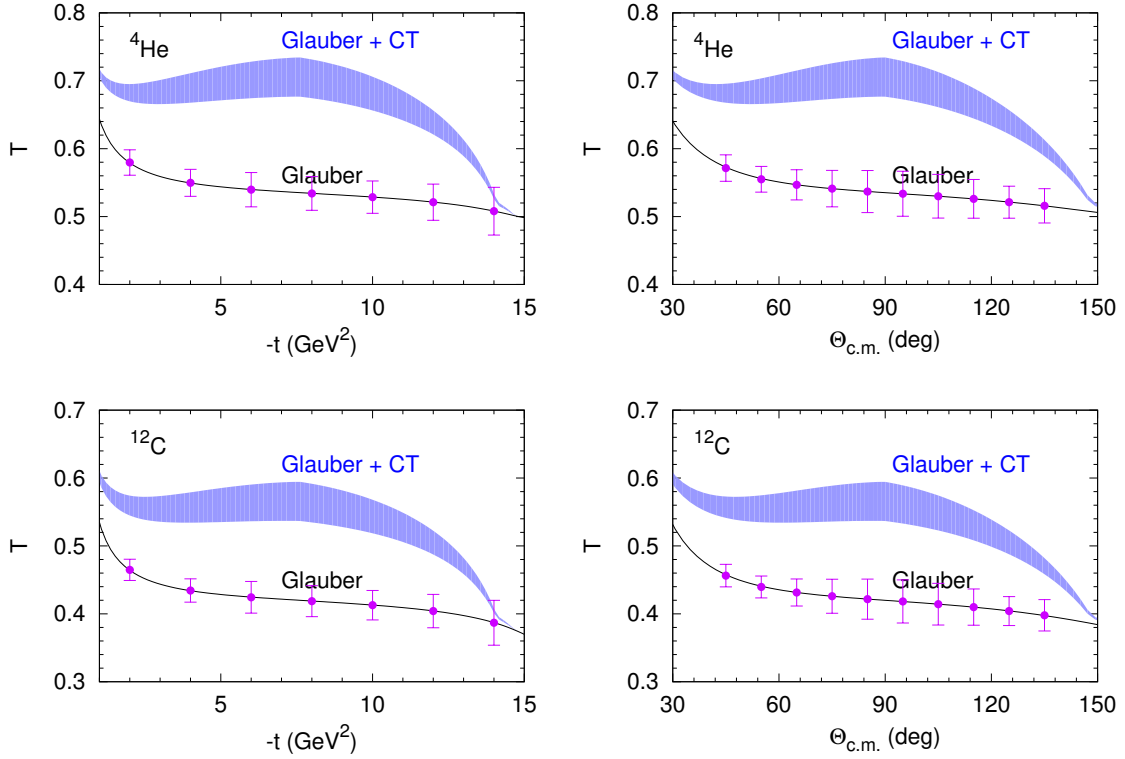


Figure 25: Expected uncertainties (statistical + systematic) for the measurement of the  $\gamma + n \rightarrow \pi^- + p$  reaction off  $^4\text{He}$  (upper row), and  $^{12}\text{C}$  (lower row).

uncertainties and are dominated by the beam flux and target densities. Both are expected to be known to better than 3% which is what we assume for the overall systematical uncertainty which is included in Fig. 25.

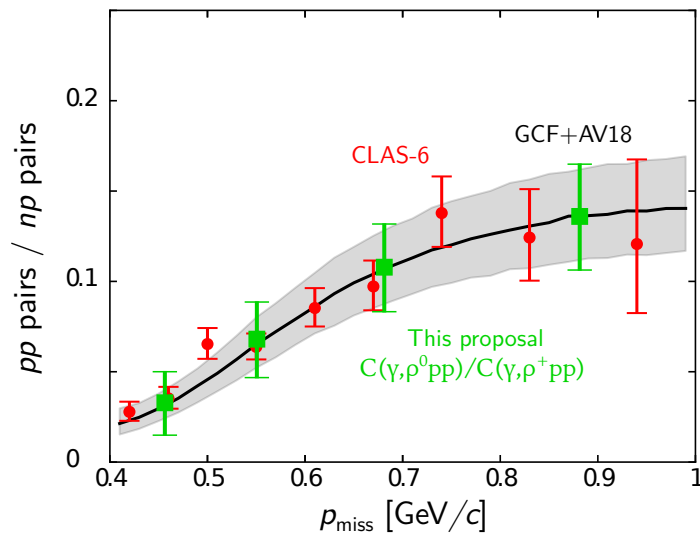


Figure 26: The expected precision of this proposal for testing  $np$ -dominance via the  $\rho$  production channel, compared with electron scattering data from CLAS-6.

For SRC studies, while the rates are modest, they are in fact comparable and even higher per reaction as compared to the 6 GeV measurements done in Hall A and B. Therefore, the cross-section ratios for scattering off nuclei relative to deuterium, in SRC kinematics, will allow us to test the observed  $np$ -dominance and extract the relative number of SRC pairs in the measured nuclei with  $< 4\%$ – $10\%$  accuracy, depending on the channel considered. As an example, Fig. 26 shows the expected sensitivity for  $\rho$ -production, the highest-rate channel, compared with the preliminary analysis of CLAS data (shown previously in Fig. 3). The precision will be sufficient to confirm both  $np$ -dominance and explore the transition to the repulsive core. These data will therefore improve our understanding of SRCs and help to reduce interpretation uncertainty in a unique way unmatched by any other measurement that can be performed at JLab.

## 6 Complementary Experiments at JLab

The goals of our proposed measurement run complementary to those of several other approved JLab 12 GeV experiments, which will be described in this section.

Semi-inclusive and exclusive measurements of short-range correlations are the focus of several recent and upcoming experiments, which are complimentary to our proposed SRC program. The Hall A experiment E12-14-011 [96] ran in 2018, measuring asymmetries between the mirror nuclei  ${}^3\text{H}$  and  ${}^3\text{He}$  to study the isospin-dependent effects in SRCs [21], along with an inclusive counterpart, E12-11-112 [97]. The Hall C experiment E12-17-005 [98] will also look for isospin-dependent effects through measurements on  ${}^{40}\text{Ca}$ ,  ${}^{48}\text{Ca}$ , and  ${}^{54}\text{Fe}$ . The Hall B run group proposal E12-17-006 includes measurements of short range correlations in a wide range of targets [99].

The interpretation of the above experiments depends on the general framework for our understanding of SRCs, FSIs, and reaction mechanisms in electron-induced pair break-up, which our proposed measurement will attempt to validate with the new method of photo-induced reactions.

Understanding of the modification of nucleon structure within the nuclear medium is a salient topic in nuclear physics under active investigation in several JLab experiments. Our proposal focuses

on a completely novel observable, branching ratio modification, which would complement traditional “EMC” electron-scattering measurements. Among the upcoming electron scattering measurements, we highlight E12-11-003A [100] and E12-11-107 [101], which will test the role that highly-virtual nucleons play in the EMC effect by looking at recoil-tagged  $F_2$  structure functions of bound nucleons in deuterium.

Color transparency for mesons, hints of which were seen in the JLab 6 GeV program [86], will be studied at high- $Q^2$  in two 12 GeV electron scattering experiments: E12-06-106 [93] (upcoming) and E12-06-107 [84] (under analysis). While these experiments are complementary to our proposed CT measurement, we point out that our measurement is sensitive to CT for baryons as well. The large number of different final states we consider will allow us to map out the spin and isospin dependence of CT.

E12-06-107 will also measure color transparency in for protons, which complements our baryonic CT measurements. A significant difference between this measurement and ours comes from the use of photon-induced reactions, which will generally have larger energy transfer (and thus greater “freezing” of PLCs) than the majority of the kinematic space probed by E12-06-107.

As discussed in section 4, the theoretical framework of PLCs suggests that both color transparency and the EMC effect have a common origin. Both these experiments and our proposed measurement will have complimentary roles in constraining that framework and in understanding the origin of the EMC effect.

## 7 Summary

We propose a 30-day measurement using the real photon beam in Hall D,  $d$ ,  $^4\text{He}$  and  $^{12}\text{C}$  targets, with the GlueX detector in its standard configuration, with the goal of studying short-range correlations, transparency and bound nucleon structure in nuclei. The use of a real photon beam as a probe provides an outstanding handle on reaction mechanism effects in SRC pair breakup, which complement the successful electron-scattering SRC program in Halls A and B. We project count rates that exceed those of the 6 GeV-era SRC experiments, allowing definitive measurements of SRC properties, the short-distance  $NN$  interaction, in-medium modification, and nuclear transparency.

## References

- [1] R. Hofstadter, “Electron scattering and nuclear structure,” *Rev. Mod. Phys.*, vol. 28, pp. 214–254, 1956.
- [2] T. De Forest, Jr. and J. D. Walecka, “Electron scattering and nuclear structure,” *Adv. Phys.*, vol. 15, pp. 1–109, 1966.
- [3] J. J. Kelly, “Nucleon knockout by intermediate-energy electrons,” *Adv. Nucl. Phys.*, vol. 23, pp. 75–294, 1996. [,75(1996)].
- [4] L. Lapikas, “Quasi-elastic electron scattering off nuclei,” *Nucl. Phys.*, vol. A553, pp. 297c–308c, 1993.
- [5] W. H. Dickhoff and C. Barbieri, “Selfconsistent Green’s function method for nuclei and nuclear matter,” *Prog. Part. Nucl. Phys.*, vol. 52, pp. 377–496, 2004.
- [6] O. Hen, G. A. Miller, E. Piassetzky, and L. B. Weinstein, “Nucleon-Nucleon Correlations, Short-lived Excitations, and the Quarks Within,” *Rev. Mod. Phys.*, vol. 89, no. 4, p. 045002, 2017.

- [7] C. Ciofi degli Atti, “In-medium short-range dynamics of nucleons: Recent theoretical and experimental advances,” *Phys. Rept.*, vol. 590, pp. 1–85, 2015.
- [8] J. Arrington, D. W. Higinbotham, G. Rosner, and M. Sargsian, “Hard probes of short-range nucleon-nucleon correlations,” *Prog. Part. Nucl. Phys.*, vol. 67, pp. 898–938, 2012.
- [9] L. Frankfurt, M. Sargsian, and M. Strikman, “Recent observation of short range nucleon correlations in nuclei and their implications for the structure of nuclei and neutron stars,” *Int. J. Mod. Phys. A*, vol. 23, pp. 2991–3055, 2008.
- [10] S. Paschalis, M. Petri, A. O. Macchiavelli, O. Hen, and E. Piassetzky, “Nucleon-nucleon correlations and the single-particle strength in atomic nuclei,” 2018.
- [11] B. Schmookler *et al.*, “Modified structure of protons and neutrons in correlated pairs,” *Nature*, vol. 566, no. 7744, pp. 354–358, 2019.
- [12] M. Duer *et al.*, “Probing high-momentum protons and neutrons in neutron-rich nuclei,” *Nature*, vol. 560, no. 7720, pp. 617–621, 2018.
- [13] O. Hen *et al.*, “Momentum sharing in imbalanced Fermi systems,” *Science*, vol. 346, pp. 614–617, 2014.
- [14] R. Subedi *et al.*, “Probing Cold Dense Nuclear Matter,” *Science*, vol. 320, pp. 1476–1478, 2008.
- [15] R. Shneor *et al.*, “Investigation of proton-proton short-range correlations via the  $^{12}\text{C}(e, e'pp)$  reaction,” *Phys. Rev. Lett.*, vol. 99, p. 072501, 2007.
- [16] I. Korover *et al.*, “Probing the Repulsive Core of the Nucleon-Nucleon Interaction via the  $^4\text{He}(e, e'pN)$  Triple-Coincidence Reaction,” *Phys. Rev. Lett.*, vol. 113, no. 2, p. 022501, 2014.
- [17] M. Duer *et al.*, “Direct Observation of Proton-Neutron Short-Range Correlation Dominance in Heavy Nuclei,” *Phys. Rev. Lett.*, vol. 122, no. 17, p. 172502, 2019.
- [18] E. O. Cohen *et al.*, “Center of Mass Motion of Short-Range Correlated Nucleon Pairs studied via the  $A(e, e'pp)$  Reaction,” *Phys. Rev. Lett.*, vol. 121, no. 9, p. 092501, 2018.
- [19] O. Hen *et al.*, “Measurement of transparency ratios for protons from short-range correlated pairs,” *Phys. Lett.*, vol. B722, pp. 63–68, 2013.
- [20] M. Duer *et al.*, “Measurement of Nuclear Transparency Ratios for Protons and Neutrons,” 2018.
- [21] R. Cruz-Torres *et al.*, “Comparing proton momentum distributions in  $A = 3$  nuclei via  $^3\text{He}$  and  $^3\text{H}(e, e'p)$  measurements,” 2019.
- [22] E. Piassetzky, M. Sargsian, L. Frankfurt, M. Strikman, and J. W. Watson, “Evidence for the strong dominance of proton-neutron correlations in nuclei,” *Phys. Rev. Lett.*, vol. 97, p. 162504, 2006.
- [23] A. Tang *et al.*, “ $n$ - $p$  short range correlations from  $(p, 2p + n)$  measurements,” *Phys. Rev. Lett.*, vol. 90, p. 042301, 2003.
- [24] R. Schiavilla, R. B. Wiringa, S. C. Pieper, and J. Carlson, “Tensor Forces and the Ground-State Structure of Nuclei,” *Phys. Rev. Lett.*, vol. 98, p. 132501, 2007.

- [25] M. M. Sargsian, T. V. Abrahamyan, M. I. Strikman, and L. L. Frankfurt, “Exclusive electro-disintegration of  ${}^3\text{He}$  at high  $Q^2$ . II. Decay function formalism,” *Phys. Rev. C*, vol. 71, p. 044615, 2005.
- [26] M. Alvioli, C. Ciofi degli Atti, and H. Morita, “Proton-neutron and proton-proton correlations in medium-weight nuclei and the role of the tensor force,” *Phys. Rev. Lett.*, vol. 100, p. 162503, 2008.
- [27] M. M. Sargsian, “New properties of the high-momentum distribution of nucleons in asymmetric nuclei,” *Phys. Rev. C*, vol. 89, no. 3, p. 034305, 2014.
- [28] J. Ryckebusch, W. Cosyn, S. Stevens, C. Casert, and J. Nys, “The isospin and neutron-to-proton excess dependence of short-range correlations,” *Phys. Lett.*, vol. B792, pp. 21–28, 2019.
- [29] L. B. Weinstein, E. Piassetzky, D. W. Higinbotham, J. Gomez, O. Hen, and R. Shneur, “Short Range Correlations and the EMC Effect,” *Phys. Rev. Lett.*, vol. 106, p. 052301, 2011.
- [30] O. Hen, E. Piassetzky, and L. B. Weinstein, “New data strengthen the connection between Short Range Correlations and the EMC effect,” *Phys. Rev.*, vol. C85, p. 047301, 2012.
- [31] O. Hen, D. W. Higinbotham, G. A. Miller, E. Piassetzky, and L. B. Weinstein, “The EMC Effect and High Momentum Nucleons in Nuclei,” *Int. J. Mod. Phys. E*, vol. 22, p. 1330017, 2013.
- [32] D. W. Higinbotham, G. Miller, O. Hen, and K. Rith, “The EMC effect still puzzles after 30 years,” *CERN Cour.*, p. 35, April 2013.
- [33] R. Cruz-Torres, A. Schmidt, G. A. Miller, L. B. Weinstein, N. Barnea, R. Weiss, E. Piassetzky, and O. Hen, “Short range correlations and the isospin dependence of nuclear correlation functions,” *Phys. Lett.*, vol. B785, pp. 304–308, 2018.
- [34] M. Kortelainen, O. Civitarese, J. Suhonen, and J. Toivanen, “Short-range correlations and neutrinoless double beta decay,” *Phys. Lett.*, vol. B647, pp. 128–132, 2007.
- [35] M. Kortelainen and J. Suhonen, “Improved short-range correlations and 0 neutrino beta beta nuclear matrix elements of Ge-76 and Se-82,” *Phys. Rev.*, vol. C75, p. 051303, 2007.
- [36] M. Kortelainen and J. Suhonen, “Nuclear matrix elements of neutrinoless double beta decay with improved short-range correlations,” *Phys. Rev.*, vol. C76, p. 024315, 2007.
- [37] J. Menendez, A. Poves, E. Caurier, and F. Nowacki, “Disassembling the Nuclear Matrix Elements of the Neutrinoless  $\beta\beta$  Decay,” *Nucl. Phys.*, vol. A818, pp. 139–151, 2009.
- [38] F. Simkovic, A. Faessler, H. Muther, V. Rodin, and M. Stauf, “The  $0\nu\beta\beta$ -decay nuclear matrix elements with self-consistent short-range correlations,” *Phys. Rev.*, vol. C79, p. 055501, 2009.
- [39] J. Engel and G. Hagen, “Corrections to the Neutrinoless Double-Beta-Decay Operator in the Shell Model,” *Phys. Rev.*, vol. C79, p. 064317, 2009.
- [40] R. Weiss, A. Schmidt, G. A. Miller, and N. Barnea, “Short-range correlations and the charge density,” *Phys. Lett.*, vol. B790, pp. 484–489, 2019.
- [41] O. Hen, B.-A. Li, W.-J. Guo, L. B. Weinstein, and E. Piassetzky, “Symmetry Energy of Nucleonic Matter With Tensor Correlations,” *Phys. Rev. C*, vol. 91, no. 2, p. 025803, 2015.
- [42] B.-J. Cai and B.-A. Li, “Effects of short-range correlations on nuclear symmetry energy within a modified Gogny-Hartree-Fock energy density functional approach,” *arXiv:nucl-th/1703.08743*, 2017.

- [43] A. Ali *et al.*, “Future Physics in Hall D with the GlueX Detector.” GlueX-doc 3870 v11, 2019.
- [44] T. De Forest, “Off-Shell electron Nucleon Cross-Sections. The Impulse Approximation,” *Nucl. Phys.*, vol. A392, pp. 232–248, 1983.
- [45] L. L. Frankfurt and M. I. Strikman, “Hard Nuclear Processes and Microscopic Nuclear Structure,” *Phys. Rept.*, vol. 160, pp. 235–427, 1988.
- [46] C. Colle, W. Cosyn, and J. Ryckebusch, “Final-state interactions in two-nucleon knockout reactions,” *Phys. Rev.*, vol. C93, no. 3, p. 034608, 2016.
- [47] M. M. Sargsian, “Selected topics in high energy semiexclusive electronuclear reactions,” *Int. J. Mod. Phys.*, vol. E10, pp. 405–458, 2001.
- [48] S. N. More, S. K. Bogner, and R. J. Furnstahl, “Scale dependence of deuteron electrodisintegration,” *Phys. Rev.*, vol. C96, no. 5, p. 054004, 2017.
- [49] J. Carlson, S. Gandolfi, F. Pederiva, S. C. Pieper, R. Schiavilla, K. E. Schmidt, and R. B. Wiringa, “Quantum Monte Carlo methods for nuclear physics,” *Rev. Mod. Phys.*, vol. 87, p. 1067, 2015.
- [50] R. Weiss, R. Cruz-Torres, N. Barnea, E. Piassetzky, and O. Hen, “The nuclear contacts and short range correlations in nuclei,” *Phys. Lett.*, vol. B780, pp. 211–215, 2018.
- [51] R. Weiss, I. Korover, E. Piassetzky, O. Hen, and N. Barnea, “Energy and momentum dependence of nuclear short-range correlations - Spectral function, exclusive scattering experiments and the contact formalism,” *Phys. Lett.*, vol. B791, pp. 242–248, 2019.
- [52] R. Weiss, B. Bazak, and N. Barnea, “Generalized nuclear contacts and momentum distributions,” *Phys. Rev.*, vol. C92, no. 5, p. 054311, 2015.
- [53] C. Ciofi degli Atti and S. Simula, “Realistic model of the nucleon spectral function in few and many nucleon systems,” *Phys. Rev. C*, vol. 53, p. 1689, 1996.
- [54] C. Colle, W. Cosyn, J. Ryckebusch, and M. Vanhalst, “Factorization of exclusive electron-induced two-nucleon knockout,” *Phys. Rev. C*, vol. 89, no. 2, p. 024603, 2014.
- [55] R. B. Wiringa, R. Schiavilla, S. C. Pieper, and J. Carlson, “Nucleon and nucleon-pair momentum distributions in  $A \leq 12$  nuclei,” *Phys. Rev. C*, vol. 89, no. 2, p. 024305, 2014.
- [56] R. B. Wiringa, V. G. J. Stoks, and R. Schiavilla, “An Accurate nucleon-nucleon potential with charge independence breaking,” *Phys. Rev.*, vol. C51, pp. 38–51, 1995.
- [57] A. Gezerlis, I. Tews, E. Epelbaum, S. Gandolfi, K. Hebeler, A. Nogga, and A. Schwenk, “Quantum Monte Carlo Calculations with Chiral Effective Field Theory Interactions,” *Phys. Rev. Lett.*, vol. 111, no. 3, p. 032501, 2013.
- [58] T. Neff and H. Feldmeier, “The Wigner function and short-range correlations in the deuteron,” 2016.
- [59] J.-W. Chen, W. Detmold, J. E. Lynn, and A. Schwenk, “Short Range Correlations and the EMC Effect in Effective Field Theory,” *Phys. Rev. Lett.*, vol. 119, no. 26, p. 262502, 2017.
- [60] C. Ciofi degli Atti, L. L. Frankfurt, L. P. Kaptari, and M. I. Strikman, “On the dependence of the wave function of a bound nucleon on its momentum and the EMC effect,” *Phys. Rev.*, vol. C76, p. 055206, 2007.

- [61] S. A. Kulagin and R. Petti, “Structure functions for light nuclei,” *Phys. Rev. C*, vol. 82, p. 054614, 2010.
- [62] C. Colle, O. Hen, W. Cosyn, I. Korover, E. Piassetzky, J. Ryckebusch, and L. B. Weinstein, “Extracting the mass dependence and quantum numbers of short-range correlated pairs from  $A(e, e'p)$  and  $A(e, e'pp)$  scattering,” *Phys. Rev.*, vol. C92, no. 2, p. 024604, 2015.
- [63] L. L. Frankfurt, M. I. Strikman, D. B. Day, and M. Sargsian, “Evidence for short range correlations from high  $Q^2$  ( $e, e'$ ) reactions,” *Phys. Rev.*, vol. C48, pp. 2451–2461, 1993.
- [64] K. S. Egiyan *et al.*, “Observation of nuclear scaling in the  $A(e, e')$  reaction at  $x_B$  greater than 1,” *Phys. Rev. C*, vol. 68, p. 014313, 2003.
- [65] K. S. Egiyan *et al.*, “Measurement of 2- and 3-nucleon short range correlation probabilities in nuclei,” *Phys. Rev. Lett.*, vol. 96, p. 082501, 2006.
- [66] N. Fomin *et al.*, “New measurements of high-momentum nucleons and short-range structures in nuclei,” *Phys. Rev. Lett.*, vol. 108, p. 092502, 2012.
- [67] L. L. Frankfurt and M. I. Strikman, “Point-like Configurations in Hadrons and Nuclei and Deep Inelastic Reactions with Leptons: EMC and EMC-like Effects,” *Nucl. Phys. B*, vol. 250, pp. 143–176, 1985.
- [68] M. R. Frank, B. K. Jennings, and G. A. Miller, “The Role of color neutrality in nuclear physics: Modifications of nucleonic wave functions,” *Phys. Rev. C*, vol. 54, pp. 920–935, 1996.
- [69] E. M. Aitala *et al.*, “Direct measurement of the pion valence quark momentum distribution, the pion light cone wave function squared,” *Phys. Rev. Lett.*, vol. 86, pp. 4768–4772, 2001.
- [70] L. Frankfurt, G. A. Miller, and M. Strikman, “Coherent nuclear diffractive production of mini-jets: Illuminating color transparency,” *Phys. Lett. B*, vol. 304, pp. 1–7, 1993.
- [71] G. R. Farrar, H. Liu, L. L. Frankfurt, and M. I. Strikman, “Transparency in Nuclear Quasiexclusive Processes with Large Momentum Transfer,” *Phys. Rev. Lett.*, vol. 61, pp. 686–689, 1988.
- [72] B. K. Jennings and G. A. Miller, “On Color Transparency,” *Phys. Lett. B*, vol. 236, pp. 209–213, 1990.
- [73] B. K. Jennings and G. A. Miller, “Color transparency: The Wherefore and the why,” *Phys. Rev. D*, vol. 44, pp. 692–703, 1991.
- [74] B. K. Jennings and G. A. Miller, “Realistic hadronic matrix element approach to color transparency,” *Phys. Rev. Lett.*, vol. 69, pp. 3619–3622, 1992.
- [75] A. S. Carroll *et al.*, “Nuclear Transparency to Large Angle  $pp$  Elastic Scattering,” *Phys. Rev. Lett.*, vol. 61, pp. 1698–1701, 1988.
- [76] I. Mardor *et al.*, “Nuclear transparency in large momentum transfer quasielastic scattering,” *Phys. Rev. Lett.*, vol. 81, pp. 5085–5088, 1998.
- [77] A. Leksanov *et al.*, “Energy dependence of nuclear transparency in  $C(p, 2p)$  scattering,” *Phys. Rev. Lett.*, vol. 87, p. 212301, 2001.
- [78] J. Aclander *et al.*, “Nuclear transparency in  $90^\circ_{\text{c.m.}}$  quasielastic  $A(p, 2p)$  reactions,” *Phys. Rev. C*, vol. 70, p. 015208, 2004.

- [79] N. Makins *et al.*, “Momentum transfer dependence of nuclear transparency from the quasielastic  $^{12}\text{C}(e, e'p)$  reaction,” *Phys. Rev. Lett.*, vol. 72, pp. 1986–1989, 1994.
- [80] T. G. O’Neill *et al.*, “ $A$ -dependence of nuclear transparency in quasielastic  $A(e, e'p)$  at high  $Q^2$ ,” *Phys. Lett. B*, vol. 351, pp. 87–92, 1995.
- [81] D. Abbott *et al.*, “Quasifree  $(e, e'p)$  reactions and proton propagation in nuclei,” *Phys. Rev. Lett.*, vol. 80, pp. 5072–5076, 1998.
- [82] K. Garrow *et al.*, “Nuclear transparency from quasielastic  $A(e, e'p)$  reactions up to  $Q^2 = 8.1(\text{GeV}/c)^2$ ,” *Phys. Rev. C*, vol. 66, p. 044613, 2002.
- [83] S. Frullani and J. Mougey, “Single-particle properties of nuclei through  $(e, e'p)$  reactions,” *Advances in Nuclear Physics*, vol. 14, 1984.
- [84] D. Dutta *et al.*, “Jefferson Lab 12 GeV experiment E12-06-107.” <https://misportal.jlab.org/mis/physics/experiments/viewProposal.cfm?paperId=686>.
- [85] B. Blaettel, G. Baym, L. L. Frankfurt, and M. Strikman, “How transparent are hadrons to pions?,” *Phys. Rev. Lett.*, vol. 70, pp. 896–899, 1993.
- [86] B. Clasie *et al.*, “Measurement of Nuclear Transparency for the  $A(e, e' \pi^+)$  Reaction,” *Phys. Rev. Lett.*, vol. 99, p. 242502, 2007.
- [87] A. Larson, G. A. Miller, and M. Strikman, “Pionic Color Transparency,” *Phys. Rev. C*, vol. 74, p. 018201, 2006.
- [88] W. Cosyn, M. C. Martinez, J. Ryckebusch, and B. Van Overmeire, “Nuclear transparencies from photoinduced pion production,” *Phys. Rev. C*, vol. 74, p. 062201, 2006.
- [89] M. M. Kaskulov, K. Gallmeister, and U. Mosel, “Pionic transparency in semi-exclusive electroproduction off nuclei,” *Phys. Rev. C*, vol. 79, p. 015207, 2009.
- [90] L. El Fassi *et al.*, “Evidence for the onset of color transparency in  $\rho^0$  electroproduction off nuclei,” *Phys. Lett. B*, vol. 712, pp. 326–330, 2012.
- [91] L. Frankfurt, G. A. Miller, and M. Strikman, “Color Transparency in Semi-Inclusive Electroproduction of rho Mesons,” *Phys. Rev. C*, vol. 78, p. 015208, 2008.
- [92] K. Gallmeister, M. Kaskulov, and U. Mosel, “Color transparency in hadronic attenuation of  $\rho^0$  mesons,” *Phys. Rev. C*, vol. 83, p. 015201, 2011.
- [93] K. Hafidi *et al.*, “Jefferson Lab 12 GeV experiment E12-06-106.” <https://misportal.jlab.org/mis/physics/experiments/viewProposal.cfm?paperId=685>.
- [94] D. Dutta *et al.*, “Nuclear transparency with the  $\gamma n \rightarrow \pi^- p$  process in  $^4\text{He}$ ,” *Phys. Rev. C*, vol. 68, p. 021001, 2003.
- [95] R. L. Anderson, D. Gustavson, D. Ritson, G. A. Weitsch, H. J. Halpern, R. Prepost, D. H. Tompkins, and D. E. Wiser, “Measurements of exclusive photoproduction processes at large values of  $t$  and  $u$  from 4 to 7.5 GeV,” *Phys. Rev. D*, vol. 14, p. 679, 1976.
- [96] O. Hen, L. B. Weinstein, S. Gilad, and W. Boeglin, “Proton and Neutron Momentum Distributions in  $A = 3$  Asymmetric Nuclei,” *arXiv/nuc1-ex:1410:4451*, 2014.
- [97] Arrington, J. and others, “Jefferson Lab 12 GeV experiment E12-11-112.” <http://hallaweb.jlab.org/collab/PAC/PAC38/Tritium-isospin.pdf>.

- [98] Hen, O. and others, “Jefferson Lab 12 GeV experiment E12-17-005.”  
<https://misportal.jlab.org/pacProposals/proposals/1352/attachments/98357/Proposal.pdf>.
- [99] Hen, O. and others, “Jefferson Lab 12 GeV experiment E12-17-006A.”  
[https://www.jlab.org/exp\\_prog/proposals/18/PR12-18-003.pdf](https://www.jlab.org/exp_prog/proposals/18/PR12-18-003.pdf).
- [100] Hen, O. and others, “Jefferson Lab 12 GeV experiment E12-11-003A.”  
[https://www.jlab.org/exp\\_prog/proposals/15/E12-11-003A.pdf](https://www.jlab.org/exp_prog/proposals/15/E12-11-003A.pdf).
- [101] O. Hen, L. B. Weinstein, S. Gilad, and S. A. Wood, “In Medium Nucleon Structure Functions, SRC, and the EMC effect,” *arXiv/nucl-ex:1409.1717*, 2014.

## A Integrated cross-section

To validate our simulation, we performed a back-of-the-envelope calculation of the rate of the  $\gamma+n \rightarrow \pi^- + p$  reaction. The differential cross-section for the reaction can be approximated using the following:

$$\frac{d\sigma}{dt} = C \cdot f(s) \cdot f(\cos \theta_{cm}) \approx 1.25 \cdot 10^7 \text{nb} \cdot \text{GeV}^{12} \cdot s^{-7} \cdot (1 - \cos \theta_{cm})^{-5} (1 + \cos \theta_{cm})^{-4}, \quad (6)$$

where the cross-section is in units of nb/GeV<sup>2</sup>, and  $\theta_{cm}$  is the polar scattering angle in the center of mass system.

The polar scattering angle in the center of mass system  $\theta_{cm}$  can be approximated as

$$\cos \theta_{cm} = \frac{t - m_\pi^2 + 2k_i \sqrt{k_f^2 + m_\pi^2}}{2k_i k_f}, \quad (7)$$

where  $k_i$ , and  $k_f$  are the center of mass momenta of incoming and outgoing particles:

$$k_i = \frac{s - m_p^2}{2\sqrt{s}} \quad (8)$$

$$k_f = \sqrt{\frac{(s - (m_p - m_\pi)^2) \cdot (s - (m_p + m_\pi)^2)}{4s}}. \quad (9)$$

Equation (7) shows that for  $\theta_{cm} > 41^\circ$ ,  $|t| > 2 \text{ (GeV/c)}^2$ . Mandelstam variables are interrelated as  $s + t + u = m^2$ , which means that for  $E_\gamma = 9 \text{ GeV}$  we have  $|t| > 2 \text{ (GeV/c)}^2$  and  $|u| > 2 \text{ (GeV/c)}^2$  for almost the whole range of  $\theta_{cm}$  between  $40^\circ$  and  $140^\circ$ .

The cross-section (6) in terms of  $\cos \theta_{cm}$ :

$$d\sigma = C \cdot s^{-7} \cdot f(\cos \theta_{cm}) dt = C_1 \cdot s^{-7} \cdot f(\cos \theta_{cm}) d \cos \theta_{cm}, \quad (10)$$

where  $C_1 = 1.25 \cdot 10^7 \cdot 2k_i k_f$ .

The total cross-section for  $E_\gamma = 9 \text{ GeV}$  and  $\theta_{cm}$  in the range between  $40^\circ$  and  $140^\circ$  is then about 2.1 nb. The number of expected MF events per day on a carbon target is

$$N = \sigma_{nucl} \cdot F \cdot T \cdot t \cdot \epsilon = 880, \quad (11)$$

where  $F = 2 \cdot 10^7$  photons/s - photon flux on target,  $T = 1.45 \cdot 10^{23}$  atoms/cm<sup>2</sup> - target density for <sup>12</sup>C,  $t = 24$  hours  $\cdot 3600$  s/hour - time,  $\epsilon = 0.64$  - detection efficiency, and  $\sigma_{nucl} = \sigma \cdot A/2 \cdot A^{-1/3} = 5.5$  nb - nuclear cross-section for <sup>12</sup>C. This is consistent within 20% with the simulation results (740 events/day for the <sup>12</sup>C target).